CR 160110

(NASA-CR-160110) SHUTTLE GLOBAL POSITIONING SYSTEM (GPS) DESIGN STUDY Final Report (Axiomatix, Los Angeles, Calif.) 50 p HC A03/MF A01 CSCL 17G

N79-17901

Unclas

G3/16 14177

Axiomatix

MAR 1979
RECEIVED
NASA STI FACILITY
ACCESS DEPT.

SHUTTLE GLOBAL POSITIONING SYSTEM (GPS) DESIGN STUDY

FINAL REPORT

Contract No. NAS 9-15387B

Prepared for

NASA Lyndon B. Johnson Space Center
Houston, Texas 77058

Prepared by

Peter W. Nilsen

Axiomatix
9841 Airport Boulevard, Suite 912
Los Angeles, California 90045

Axiomatix Report No. R7901-2
January 16, 1979

TABLE OF CONTENTS

		Page
LIST OF FIGURES		iii
1.0	INTRODUCTION AND SUMMARY	1
2.0	EFFECTS OF OSCILLATOR NOISE ON SHUTTLE GPS RECEIVER PERFORMANCE	3
3.0	GPS NAVIGATION SYSTEM SELF-TEST	14
4.0	GPS GROUND TRANSMITTER DESIGN TO AUGMENT SHUTTLE NAVIGATION	22
5.0	EFFECTS OF IONOSPHERIC DELAY MODELING ON GPS RECEIVER DESIGN	29
6.0	GPS RECEIVER TRACKING OF SHUTTLE TRANSIENT MANEUVERS	40
REFERENCES		46

LIST OF FIGURES

		Page
1.	Phase Lock Loop	4
2.	Mathematical Model of Nonlinear Phase Lock Loop	5
3.	Linearized Tracking Loop	5
4.	Equivalent Noise Filter	6
5.	Loop Filter	7
6.	Phase Noise Spectral Density of Low Noise 5 MHz Crystal Oscillator	10
7.	Equivalent VCO Operating at 1.575×10^9 Hz	13
8.	Single-Channel Sequential Receiver with Self-Test	16
9.	Self-Tester Functional Diagram	17
10.	Time-Multiplexing of Self-Function	19
11.	Shuttle/GPS RPA Self-Test Flow Diagram	20
12.	GPS Ground Transmitter for Shuttle Landing - Ground SAT	23
13.	GPS Inverted Range Ground Transmitter	26
14.	Ground Transmitter Block Diagram	27
15.	Error in Slab Thickness Model	33
16.	Eleven-Parameter Vertical Electron Density Profile	34
17.	APL Ionospheric Model Residuals	36
18.	Front-End and Down-Converter for Two-Frequency Receiver	38
19.	Typical RF Frequency Plan for Two-Frequency Receiver Synthesizer	39
20.	Jerk Models for Receiver Transient Performance Evaluation	41
21.	Error Response for 2nd Order Phase Lock Loop with Acceleration Rate (Jerk) Input	44
22.	GPS Receiver Tracking Loop Response to Shuttle Transient Maneuver	45

1.0 INTRODUCTION AND SUMMARY

This report documents the results of several Shuttle/GPS studies conducted by Axiomatix under Contract NAS 9-15387B for NASA's Johnson Space Center. These studies augment the studies conducted by Axiomatix for NASA under the companion contract NAS 9-15387C. Several of the investigations reported here, such as the GPS system self-test, the ground transmitter, and the ionospheric modeling investigations, grew out of needs which were developed in the Shuttle/GPS Panel meetings that Axiomatix participated in. The effects of oscillator noise and the transient maneuver analyses were conducted as part of the effort to determine the GPS receiver performance in the Shuttle environment. These studies and investigations are summarized briefly below.

The investigation of the effects of oscillator noise on the GPS receiver developed comprehensive models of the oscillator phase noise process and the phase lock loop response to phase noise. It is shown that, for a reasonably low phase noise oscillator, the degradation to Shuttle GPS receiver performance is negligible.

A Shuttle/GPS receiver self-test mode is investigated. This investigation was motivated by the desire to utilize the one good GPS receiver in the doubly redundant system in the event of one failure. A viable technique is developed that is capable of testing the GPS/Shuttle data interfaces, as well as the receiver itself.

Since the Shuttle will utilize GPS before the full constellation of 24 satellites is deployed, it may be desirable to use a GPS ground transmitter for Shuttle landing operations. Such a ground transmitter is described and a cost estimate made.

The GPS system utilizes two frequencies, L1 and L2, to correct for ionospheric delay. An investigation is performed to determine if the ionospheric delay could be modeled so that dependency on L2 might be eliminated. The conclusion is reached that this is not practical and is a poor receiver complexity trade-off.

Since the Shuttle fires thrusters to initiate maneuvers while in orbit, transients of range acceleration or jerk occur. Such transients can cause narrowband receivers to lose lock. Thus, the performance of a Shuttle/GPS receiver with typical Shuttle transient maneuvers has been

analyzed. Worst-case receiver bandwidths were used and it is shown that the receiver tracking performance is negligibly affected.

2.0 EFFECTS OF OSCILLATOR NOISE ON SHUTTLE GPS RECEIVER PERFORMANCE

Introduction

Oscillator phase noise, generally referred to as 1/f noise, degrades the doppler measurement capability of the GPS receiver and, if severe enough, can raise the receiver threshold. This latter effect can cause the receiver to lose lock prematurely, lose data, or take longer for acquisition of the PN signal. The extent of receiver degradation is dependent on the receiver carrier tracking loop bandwidth and the phase noise spectral density of the carrier. Thus, it is important to analyze the carrier (Costas) tracking loop phase error caused by 1/f noise for nominal Shuttle GPS receiver bandwidths and a typical "good" oscillator phase noise spectral density. The following analysis has thus been performed, and the results show that 1/f noise is not expected to degrade receiver tracking or data performance.

Analysis

The model of the phase locked carrier tracking loop used for the analysis is given in Figure 1, where

$$S(t) = \sqrt{2}\, A \sin\left[\omega_0 t + \theta_0(t)\right]$$

and

A = amplitude of input signal

$\theta_0(t)$ = input phase (may be constant or may represent doppler or frequency offset)

$r(t) \equiv$ reference voltage $= \sqrt{2}\, K_1 \cos\left[\omega_0 t + \hat{\theta}_0(t)\right]$

K_1 = voltage gain

$\hat{\theta}_0(t)$ = phase estimate

$\varepsilon(t)$ = dynamic phase $= K_d\, y(t)\, r(t)$ (at baseband)

$= K_d A K_1 \sin \phi(t)$

K_d = detector gain

$\phi(t) = \theta_0(t) - \hat{\theta}_0(t)$ = phase error

The VCO operation is given by

$$s\hat{\theta}_0 = K_v[z(t) + \text{a.v.}] \quad (K_v \text{ in rad/sec/volt}).$$

Assume noise = 0 and acquisition voltage (a.v.) = 0, so that

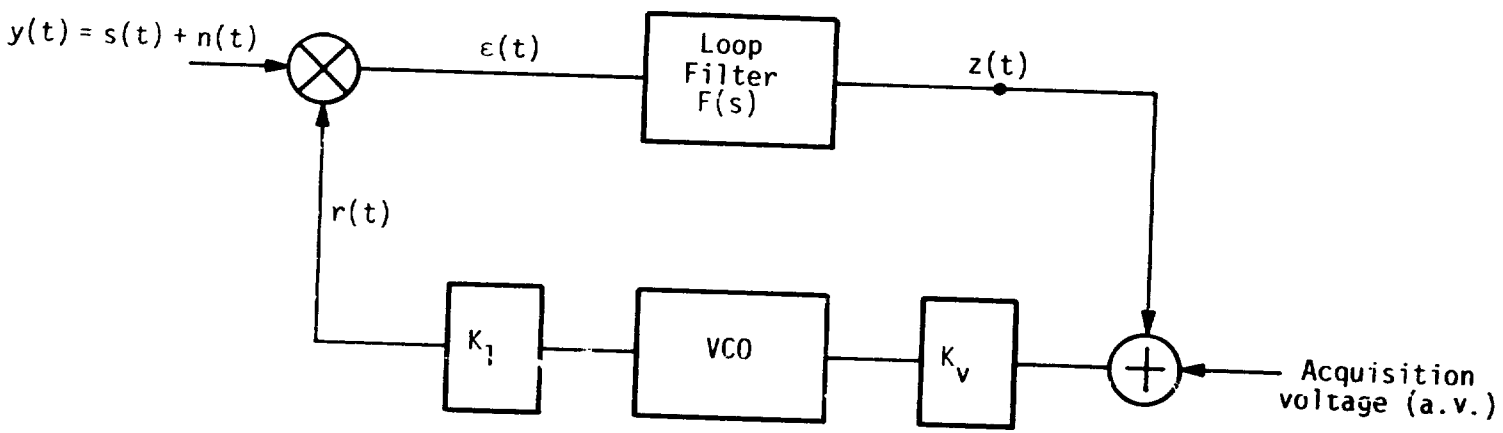

Figure 1. Phase Lock Loop

$$\theta_0 - \phi = \hat{\theta}_0 = \frac{K_v}{s} z(t) = \frac{K_v f(s)}{s} \varepsilon(s)$$

$$= A K_1 K_d K_v \frac{f(s)}{s} \sin \phi(s) .$$

Let $K \triangleq K_1 K_d K_v$ = loop gain and thus $\phi(t) = \theta_0(t) - A K f(s) \sin \phi(s)$.

$$\frac{d\phi(t)}{dt} = \frac{d\theta_0(t)}{dt} - A K \int_0^t f(t-\tau) \sin \phi(\tau)\, d\tau . \qquad (1)$$

Equation (1) is the nonlinear integral equation that represents operation of the phase lock loop. Its equivalent mathematical model is shown in Figure 2.

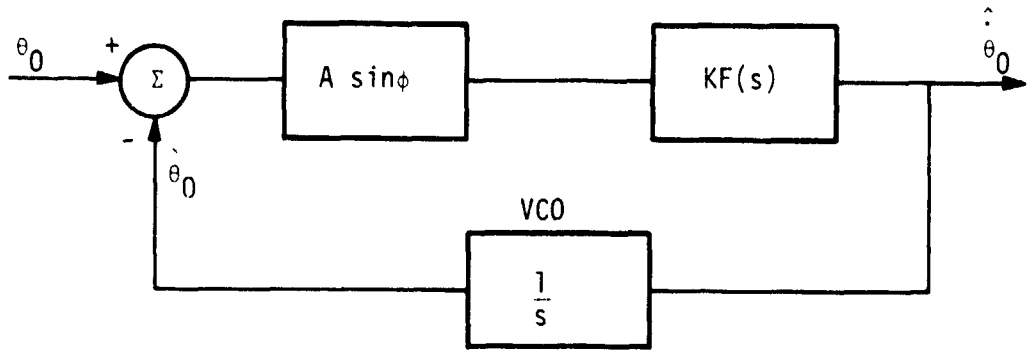

Figure 2. Mathematical Model of Nonlinear Phase Lock Loop

Assume the phase error ϕ is very small; then $\sin \phi \simeq \phi$ and the loop will be linearized and will take the form shown in Figure 3.

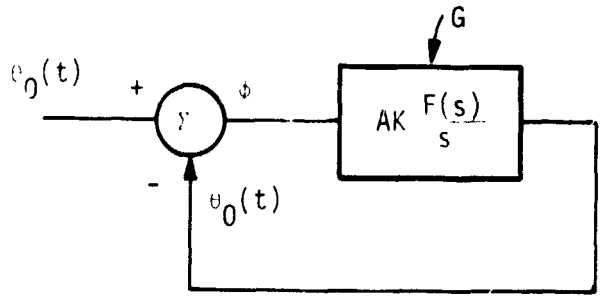

Figure 3. Linearized Tracking Loop

The linearized closed-loop transfer function $H(s) \triangleq \hat{\theta}_0(s)/\theta_0(s)$ from Figure 3 is

$$(\theta_0 - \hat{\theta}_0)\,\frac{AKf(s)}{s} = \hat{\theta}_0 .$$

Let $G = \frac{AKf(s)}{s}$; then $G\theta_0 - G\hat{\theta}_0 = \hat{\theta}_0$, $\hat{\theta}_0(1+G) = G\theta_0$, and

$$H(s) = \frac{\hat{\theta}_0}{\theta_0} = \frac{G}{1+G} = \frac{AKf(s)}{s+AKf(s)} . \tag{2}$$

The relationship between $\phi(s)$ and $\theta_0(s)$ is

$$\theta_0 - \phi G = \phi$$

$$\phi(1+G) = \theta_0$$

$$\phi = \left[1 - \frac{G}{1+G}\right]\theta_0 ,$$

and from (2),

$$\phi(s) = [1 - H(s)]\,\theta_0(s) . \tag{3}$$

The equivalent filter is shown in Figure 4.

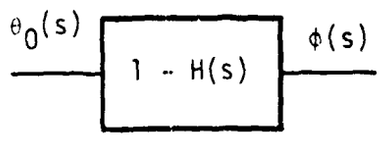

Figure 4. Equivalent Noise Filter

Assume the power spectral density of the error process $\phi(t)$ to be $S_\phi(f)$, and $S_{\theta_0}(f)$ is the power spectral density of the error process $\theta_0(t)$. Then,

$$S_\phi(f) = S_{\theta_0}(f)\,|1 - H(j\omega)|^2 . \tag{4}$$

If we assume the process $\theta_0(t)$ has a null mean value, then

$$\bar{\theta}_0(t) = \bar{\hat{\theta}}_0(t) = \bar{\phi}(t) = 0$$

and the variance of the error phase process $\phi(t)$ is

$$\sigma_\phi^2 = \int_{-\infty}^{\infty} S_{\theta_0}(f)\,|1 - H(j\omega)|^2\,df . \tag{5}$$

It is required to calculate σ_ϕ^2 using (5) under the following assumptions: The loop filter is as shown in Figure 5.

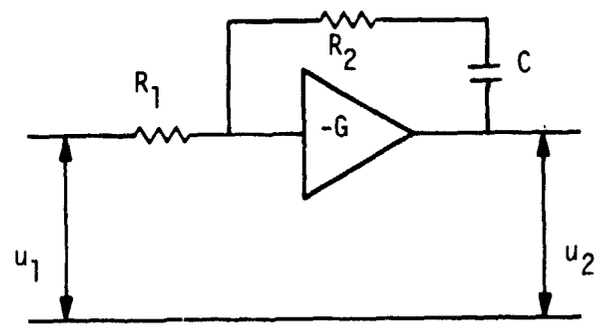

Figure 5. Loop Filter

The loop filter transfer function $F(j\omega)$ can be calculated as follows [1,2]:

$$F(j\omega) = \frac{u_2(j\omega)}{u_1(j\omega)} = -G\,\frac{1 + j\omega\,\tau_2}{1 + j\omega\,\tau_1'}\,,$$

where $\tau_2 = R_2 C$

$\tau_1' = (R_1 + GR_1 + R_2)\,C\,.$

Assume G is relatively large; then

$$\tau_1' \approx G R_1 C\,.$$

$$F(j\omega) \approx G\,\frac{1 + j\omega\,\tau_2}{1 + j\omega\,G\,R_1\,C} \approx \frac{1 + j\omega\,\tau_2}{j\omega\,R_1\,C} = \frac{1 + j\omega\,\tau_2}{j\omega\,\tau_1}\,, \tag{6}$$

where $\tau_2 = R_2 C$ and $\tau_1 = R_1 C\,.$

The natural angular frequency of the loop ω_n is always given by [1]:

$$\omega_n^{\,2} = \frac{AK}{\tau_1}\,, \tag{7}$$

and the damping constant ζ by

$$\zeta = \frac{1}{2}\,\tau_2\,\sqrt{AK/\tau_1}\,. \tag{8}$$

This implies

$$2\zeta\,\omega_n = A\,K\,\tau_2/\tau_1\,. \tag{9}$$

Substituting $F(j\omega)$ of (6) into (2) gives

$$H(j\omega) = \frac{A\,K\,(1 + j\omega\,\tau_2)}{j\omega(j\omega\,\tau_1) + A\,K\,(1 + j\omega\,\tau_2)} = \frac{AK/\tau_1 + j\omega\,AK\,\tau_2/\tau_1}{-\omega^2 + AK/\tau_1 + j\omega\,A\,K\,\tau_2/\tau_1}\,.$$

Using (7) and (9), we get:

$$H(j\omega) = \frac{\omega_n^2 + 2j\omega\zeta\omega_n}{-\omega^2 + \omega_n^2 + 2j\omega\zeta\omega_n}$$

and

$$1 - H(j\omega) = \frac{\omega_n^2 + 2j\omega\zeta\omega_n - \omega^2 - \omega_n^2 - 2j\omega\zeta\omega_n}{\omega_n^2 + 2j\omega\zeta\omega_n - \omega^2} = \frac{\omega^2}{\omega^2 - 2j\omega\zeta\omega_n - \omega_n^2}$$

$$\begin{aligned}
|1 - H(j\omega)|^2 &= (1 - H(j\omega))(1 - H(j\omega))^* \\
&= \frac{\omega^2}{\omega^2 - \omega_n^2 - 2j\omega\zeta\omega_n} \times \frac{\omega^2}{\omega^2 - \omega_n^2 + 2j\omega\zeta\omega_n} \\
&= \frac{\omega^4}{(\omega^2 - \omega_n^2)^2 + (2\omega\zeta\omega_n)^2} \\
&= \frac{\omega^4}{\omega^4 + \omega_n^4 - 2\omega^2\omega_n^2 + 4\omega^2\omega_n^2\zeta^2} .
\end{aligned}$$

Assuming $\zeta = \frac{1}{\sqrt{2}}$, we get

$$|1 - H(j\omega)|^2 = \frac{\omega^4}{\omega^4 + \omega_n^4} . \tag{10}$$

It is reasonable to assume that the oscillator phase noise spectral density $S_{\theta_0}(f)$ has the shape given in Figure 6 and denoted by $\mathcal{L}(f)$. From Figure 6, we get

$$\left.\begin{aligned}
S_{\theta_0}(f) &= \frac{10^{-11.7}}{f^3} \\
&= \frac{10^{-13.0}}{f} \\
&= 10^{-14.45}
\end{aligned}\right\} \begin{aligned} &0 \le f \le 4.3 \text{ Hz} \\ &4.3 \le f \le 30 \text{ Hz} \\ &f > 30 \text{ Hz} \end{aligned} \tag{11}$$

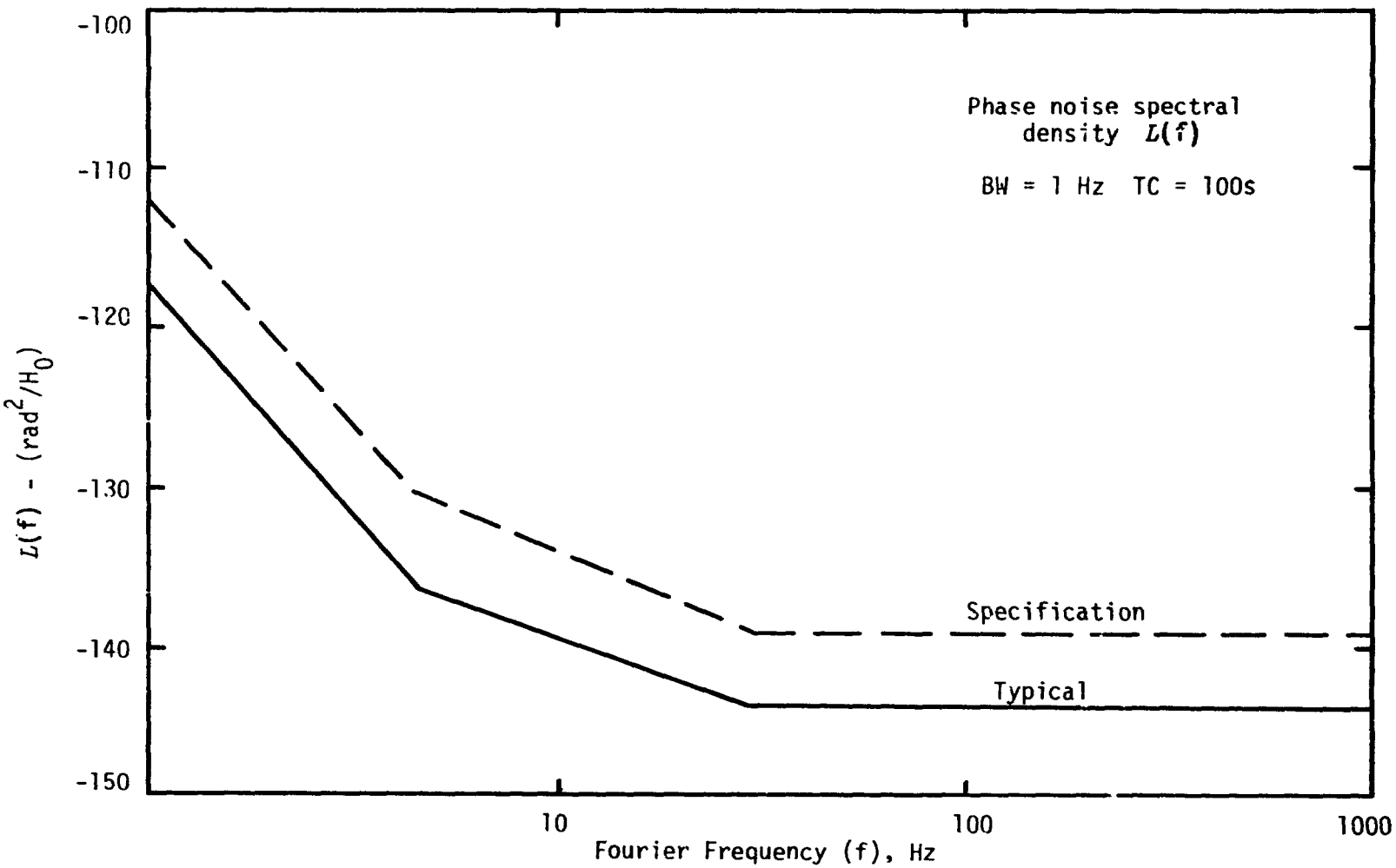

Figure 6. Phase Noise Spectral Density of Low Noise 5 MHz Crystal Oscillator

Substituting values of (10) and (11) in (5) gives

$$\sigma_\phi^2 = 2\left[\int_0^{4.3} \frac{10^{-11.7}}{f^3} \frac{\omega^4}{\omega_n^4+\omega^4}\, df + \int_{4.3}^{30} \frac{10^{-13.0}}{f} \frac{\omega^4}{\omega_n^4+\omega^4}\, df \right.$$

$$\left. + \int_{30}^{B_{IF}} 10^{-14.45} \frac{\omega^4}{\omega_n^4+\omega^4}\, df\right]$$

$$= 2[I_1 + I_2 + I_3] .$$

Equation (5), the tracking error variance, will be evaluated for a narrow-band tracking loop, representative of a code tracking loop, where $\omega_n = 2$ rad/sec, and for a wider tracking loop, $\omega_n = 30$ rad/sec, representative of the carrier tracking loop. In both cases, the receiver IF bandwidth is taken as 30 Hz.

The values of integrals I_1, I_2, and I_3 are calculated using tables of integrals [3] as follows:

$$I_1 = 10^{-11.7}(2\pi)^2 \int_0^{4.3} \frac{\omega}{\omega_n^4+\omega^4}\, 2\pi\, df = \frac{7.87698}{10^{11}} \int_0^{8.6\pi} \frac{\omega}{16+\omega^4}\, d\omega ,$$

and, from [3, p. 62],

$$\int \frac{x}{a+bx^4}\, dx = \frac{1}{2\sqrt{ab}} \tan^{-1} x^2 \sqrt{b/a} ,$$

so that

$$I_1 = \frac{7.87698}{10^{11}} \left[\frac{1}{2\times 4} \tan^{-1} (\omega^2/4)\right]_0^{8.6\pi} = 1.54\times 10^{-11} .$$

Similarly,

$$I_2 = 10^{-13.0} \int_{2\pi\times 4.3}^{2\pi\times 30} \frac{\omega^3}{16+\omega^4}\, d\omega ,$$

and from [3],

$$\int \frac{x^3}{a+bx^4}\, dx = \frac{1}{4b} \ln (a+bx^4) ,$$

$$I_2 = 10^{-13.0}\left[\frac{1}{4}\ \text{in}\ (16+\omega^4)\right]_{8.6\pi}^{60\pi} = 1.94\times 10^{-13}.$$

Likewise,

$$I_3 = 10^{-14.45}\,\frac{1}{2\pi}\int_{30}^{B_{IF}} \frac{\omega^4}{\omega_n^4+\omega^4}\,2\pi\ df$$

$$= 0.05647\times 10^{-14}\int_{60\pi}^{400\pi}\frac{\omega^4}{16+\omega^4}\,d\omega,$$

and, from [3],

$$\frac{1}{b}\int\frac{bx^4}{a+bx^4}\,dx = \frac{1}{b}\int\frac{a+bx^4-a}{a+bx^4}\,dx = \frac{1}{b}\left\{\int dx - \int\frac{a}{a+bx^4}\,dx\right\},$$

where

$$a\int\frac{1}{a+bx^4}\,dx = \frac{\sqrt[4]{a/b}}{4a\sqrt{2}}\left\{\ln\frac{x^2+\sqrt[4]{a/b}\,x\sqrt{2}+\sqrt{a/b}}{x^2-\sqrt[4]{a/b}\,x\sqrt{2}+\sqrt{a/b}} + 2\tan^{-1}\left(\frac{\sqrt[4]{a/b}\,x\sqrt{2}}{\sqrt{a/b}-x^2}\right)\right\}.$$

Thus,

$$I_3 = 0.05647\times 10^{-14}\left[\omega - \frac{1}{2\sqrt{2}}\left\{\ln\frac{\omega^2+2\sqrt{2}\,\omega+4}{\omega^2-2\sqrt{2}\,\omega+4} + 2\tan^{-1}\left(\frac{2\sqrt{2}\,\omega}{4-\omega^2}\right)\right\}\right]_{60\pi}^{400\pi}$$

$$= 6\times 10^{-14}.$$

Upon combining the three integrals, the rms tracking error is found to be

$$\sigma_\phi = 5.7\times 10^{-6}\ \text{rad}.$$

Proceeding in a similar manner, the rms error for the $\omega_n = 30$ rad/sec case is found to be 1.3×10^{-6} rad.

It is important to note that these errors are calculated for a 5 MHz oscillator.

Since the GPS L1 frequency is 1.575 GHz, the oscillator is followed by a multiplication function so that the equivalent receiver oscillator has the frequency 1.575×10^9 Hz, as shown in Figure 7,

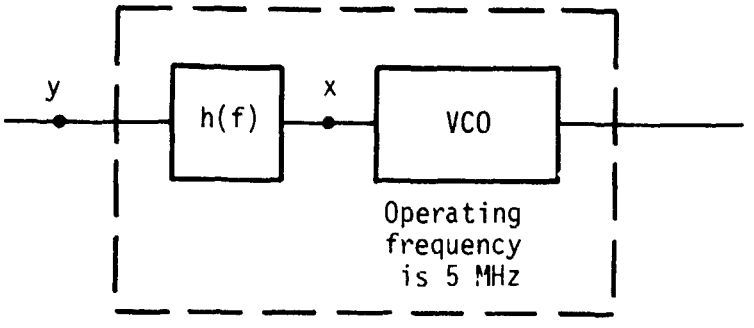

Figure 7. Equivalent VCO Operating at 1.575×10^9 Hz

where $h(f) = \dfrac{1.575 \times 10^9}{5 \times 10^6} = 315$

$$S_y(f) = |h(f)|^2 S_x(f) = (315)^2 S_x(f),$$

so a correction on error variance has to be done for both cases as follows:

<u>Case 1</u> $\omega_n = 2$ rad/sec, $B_{IF} = 200$ Hz/sec

$$\sigma_\phi^2 = 32.420793 \times 10^{-12} \times (315)^2$$

$$\sigma_\phi = 0.0017935 \text{ rad} = 0.10256 \text{ deg}.$$

<u>Case 2</u> $\omega_n = 30$ rad/sec, $B_{IF} = 200$ Hz/sec

$$\sigma_\phi^2 = 160.82877 \times 10^{-14} \times (315)^2$$

$$\sigma_\phi = 0.00039947 \text{ rad} = 0.02289 \text{ deg}.$$

Thus, it is seen that the phase error due to oscillator noise is negligible.

3.0 GPS NAVIGATION SYSTEM SELF-TEST

System self-test is a concept that enables the GPS Navigation System to validate its own performance in real time during a mission. This concept should not be confused with certain avionics Built-In Test Equipment (BITE) which is usually used to isolate processor faults to the module or board level. Also, BITE is sometimes a software function used to verify the correct operation of receiver software and firmware. An example of such a BITE function for a GPS receiver is given in Table 1.

Table 1. Sequential Receiver Built-In Test Concepts for Software/Firmware

- Power Fail/Restart Interrupt
  - Performs critical data memory validity check on restart
  - Calls system initialization on restart
  - Flag made available to distinguish fail from restart
- Computation Error Interrupts
  - Floating point microcode
  - FORTRAN library errors
  - Errors tabulated and computation continued or process restarted, depending on error
- Time-Out Error
  - Used for stack overflow, jump to restart
- Self-Test Background Task
  - AFI monitoring
  - ROM checksum
  - RAM read/store/restore/compare tests
  - Critical data memory checksum
- Each I/O Task Provides Bit Functions
  - Telemetry
  - Receiver

Since the baseline Shuttle GPS Navigation System is a two-string system, when the two GPS navigation solutions do not agree due to a malfunction in one of the strings, both are discarded and the Shuttle utilizes the baseline navigation system (i.e., TDRSS doppler, or TACAN).

An effective self-test feature would disclose which GPS receiver was still providing good navigation data and enable this data to be utilized by the Shuttle, if so desired.

The desirable features of a self-test function include the ability to provide a system end-to-end test which provides an absolute indication of the system health of the entire GPS navigation chain. This indication should be a continuous, real time, in-flight health evaluation. However, it should also be capable of being used as a maintenance tool to check out the receiver performance prior to installation in the Shuttle. Each GPS receiver should have its own self-tester, independently operated. The self-test should provide a verification of receiver "front end" health, including tracking and data functions, and pseudo range and doppler measurement functions. It is also possible to consider verification of receiver processor and memory health. This can be accomplished by a "test state vector" and "test bite" indicator which are compared in the Shuttle GPC with the correct design values.

A block diagram of a possible self-test implementation for a sequential GPS receiver is shown in Figure 8. The essence of this system is the internal generation of a GPS-like signal that the receiver processes. In processing this signal, the receiver must exercise, and thereby check out, all the functions required for normal GPS satellite signal reception. The basics of the test GPS signal generation are shown in the block diagram in Figure 9. As can be seen, the self-tester employs a GPS signal generator that modulates an L1 carrier with a P code and appropriate data stream. This signal is injected, at an appropriate RF level, as close as possible to the system antenna. The two most logical places to inject the test signal are at the preamp input and at the receiver input. The advantage of injecting the signal at the preamp input is that the entire RF circuit is tested; however, this is accomplished at the expense of an additional coax cable which must be run from the receiver to the preamp. Even though this cable can be a small-diameter, relatively lossy cable, the running of an additional cable to the preamp can present problems due to severe space limitations. Also, this signal injection at the preamp input will cause a slight increase in the preamp noise temperature.

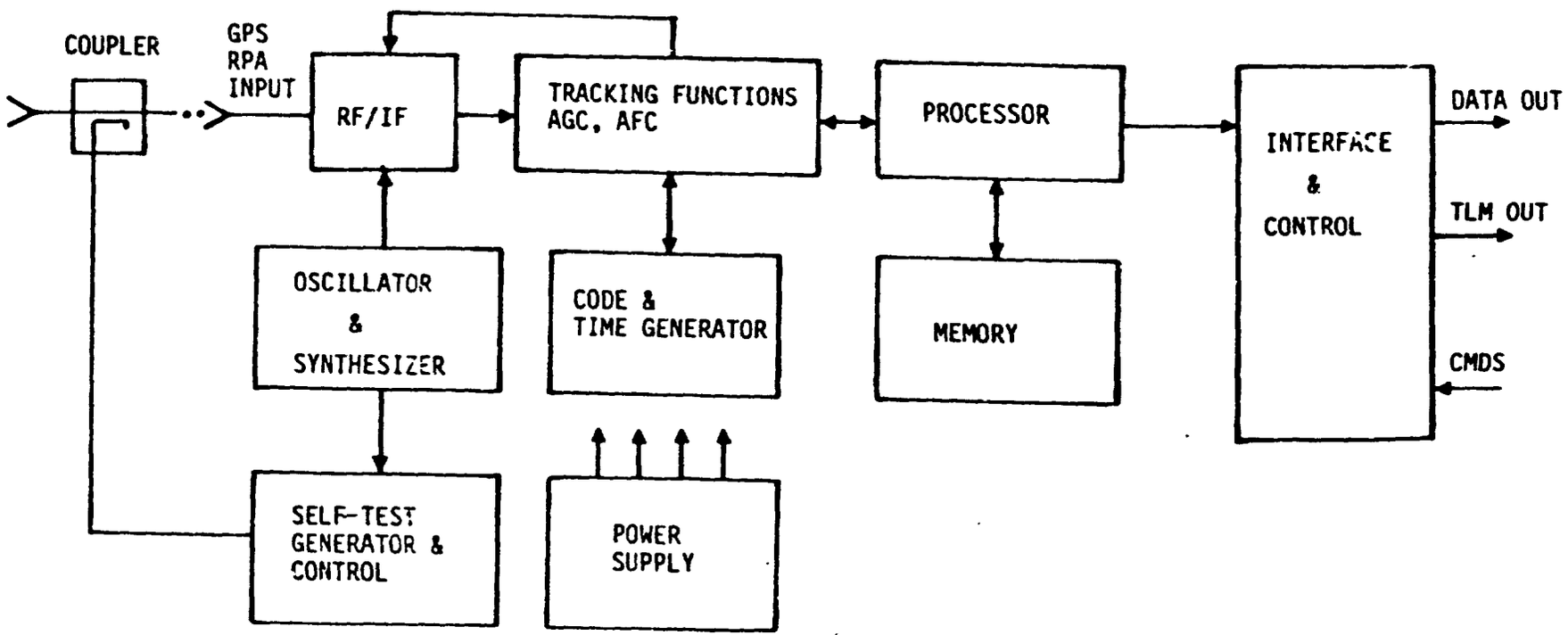

Figure 8. Single-Channel Sequential Receiver with Self-Test

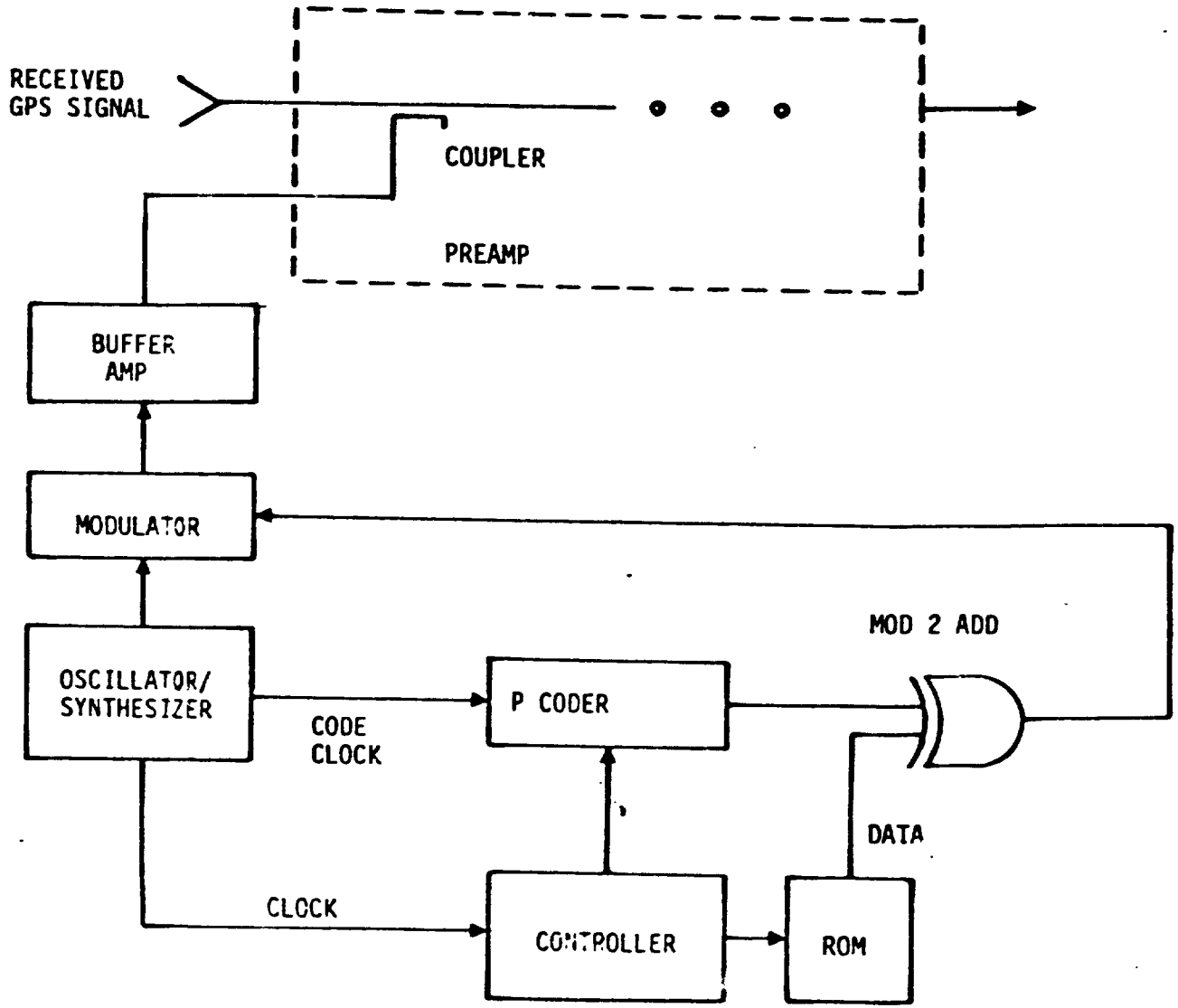

Figure 9. Self-Tester Functional Diagram

Injection of the test signal at the receiver input avoids the problem of running an extra coax cable to the vicinity of the antenna. It also avoids the additional increase in noise temperature; however, it does not provide for checking the preamp. Thus, if a preamp fails, the self-test may still indicate satisfactory operation of the system. This is not as serious a problem as it might seem since preamplifier failures are generally "hard failures" which are detected by other receiver health indicators, such as receiver AGC. Thus, it would seem that the receiver front end is a reasonable point to inject the self-test signal.

The self-test function must be automatically time-multiplexed with the normal GPS signal measurement function. This concept is illustrated in Figure 10 for a sequential receiver. Normally, the sequential receiver sequences from satellite number 1 slot to satellite number 2 slot and so on until four measurements have been completed. The sequence is then back to satellite number 1, with appropriate substitution of new satellites as they become visible. A typical frame length is no more than 24 seconds long. The test function is multiplexed by creating a fifth slot in the frame for testing. Since it is not necessary to verify system health as frequently as every 30 seconds, the fifth slot can be multiplexed itself with other processes such as search and acquisition of additional satellites. Thus, a typical sequence for slot 5 might be two frames of search for new satellites, followed by a test frame. This would provide health verification every 90 seconds or less. Slot 5 could easily be software-configurable.

A simplified flow diagram of the self-test process is shown in Figure 11. The test signal that is generated is designed such that the transmitted code phase and carrier doppler are preprogrammed to correspond to a desired range and range rate. Furthermore, the data message on the test signal would contain the ephemerides for a favorable geometrical position of the "test satellite." If it is desired to just verify receiver RF and baseband processing, only the pseudo range and delta range words and the data word need to be compared with the stored "test" words. A more complete test, however, of the receiver is to have the navigation processor portion of the receiver process the "test" pseudo range, delta range and ephemerides to calculate a "test" state vector. Since the comparison with the true value is performed in the Shuttle GPC,

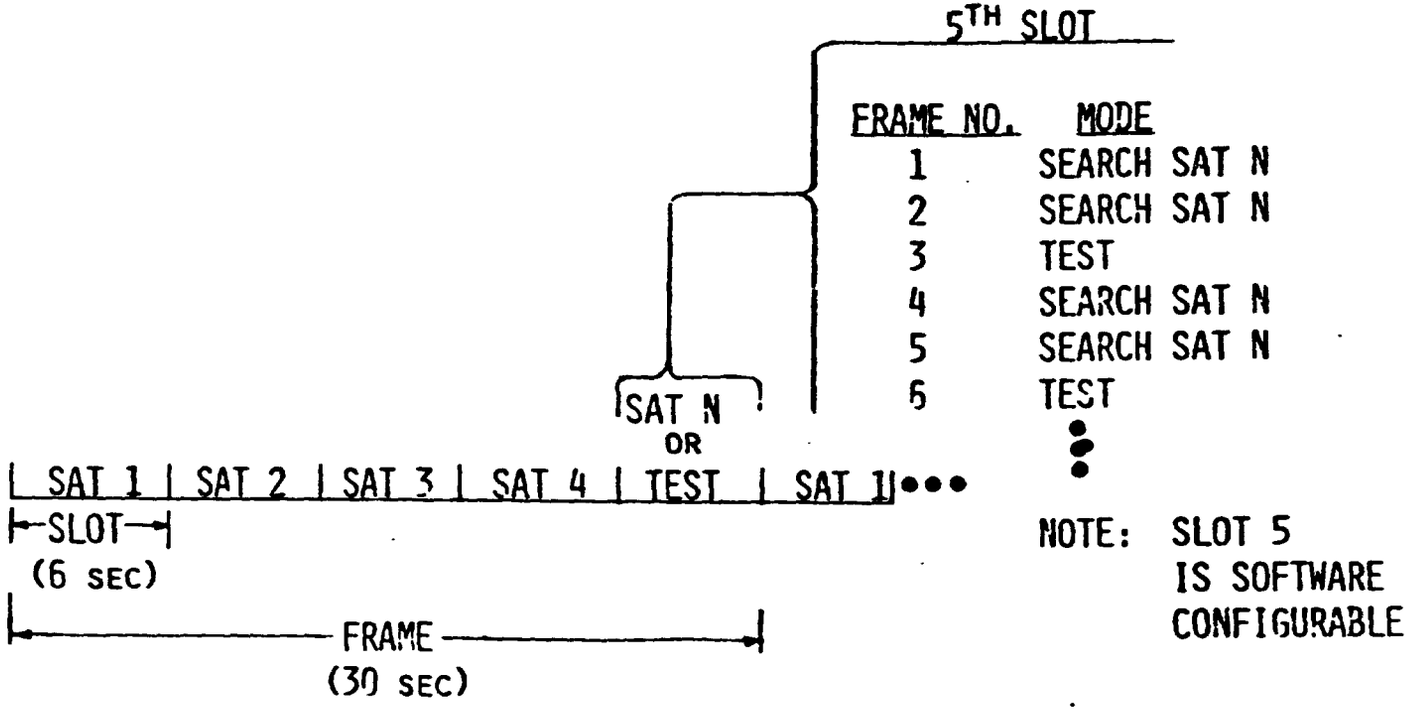

Figure 10. Time-Multiplexing of Self-Function

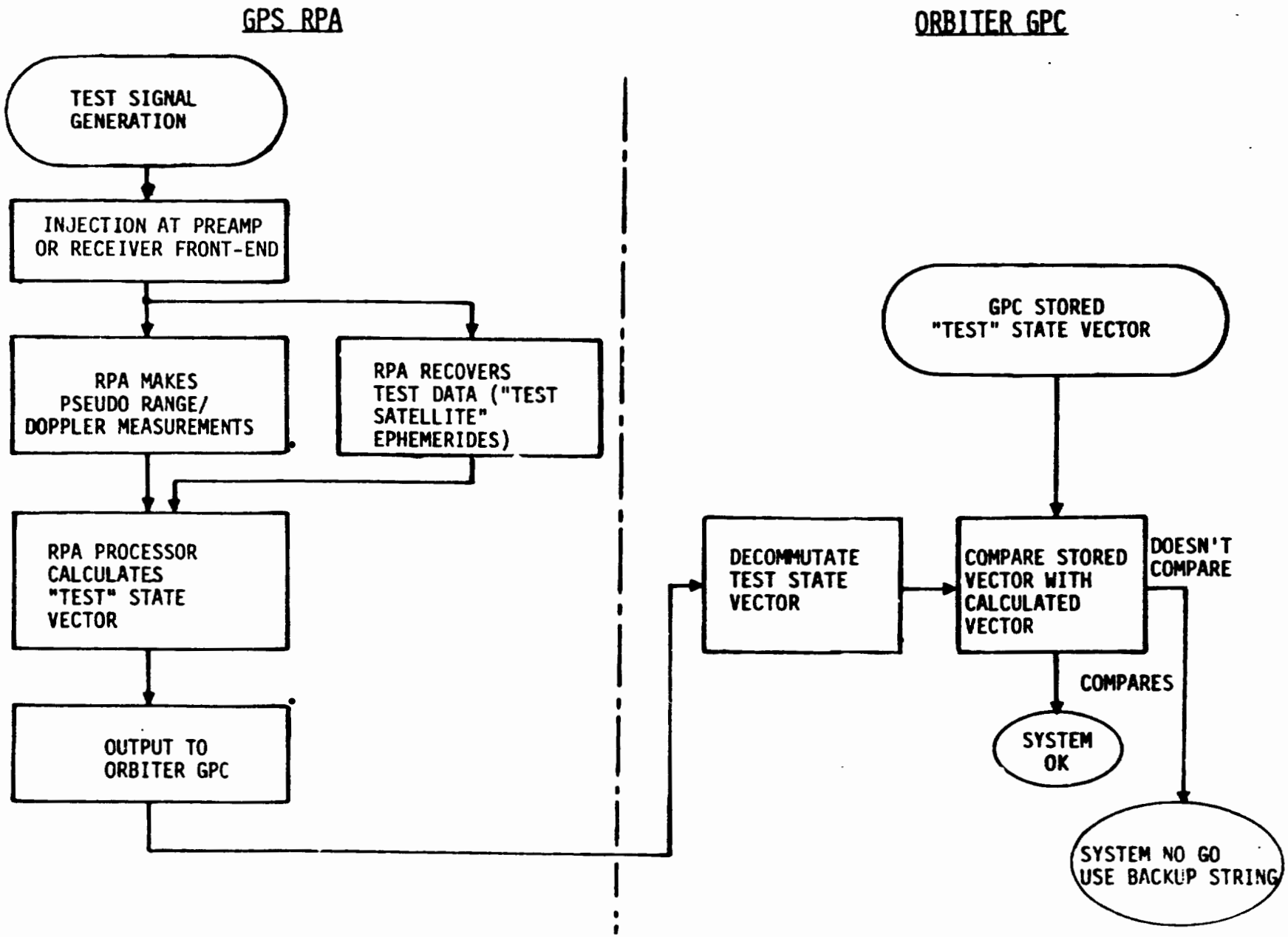

Figure 11. Shuttle/GPS RPA Self-Test Flow Diagram

this test also evaluates the GPS RPA/Shuttle data interface. This is the test that is shown in Figure 11.

4.0 GPS GROUND TRANSMITTER DESIGN TO AUGMENT SHUTTLE NAVIGATION

When the Shuttle enters the atmosphere for landing, there is a possibility of significant enhancement of the landing navigation accuracy with GPS by utilizing earth-based GPS transmitters. The earth-based GPS transmitters, hereafter referred to as ground SAT, offer a more favorable geometry for calculation of the GPS navigation solution. This is especially true for Shuttle operations prior to the fully deployed GPS 24-satellite constellation. The ground SAT would be located within approximately several hundred miles of the Shuttle landing site. This section reports the results of Axiomatix's investigation of the design, performance and cost of the ground SAT.

The function of the ground SAT is to emulate a normal GPS satellite transmission. Of course, the data message regarding the ephemerides of the ground SAT is drastically different than that of the normal GPS satellite; however, the navigation signal structure is exactly the same. A functional block diagram of a ground SAT is shown in Figure 12. The major difference between this diagram and an equivalent diagram for a normal GPS satellite is the GPS user receiver that is present in the ground SAT. This receiver is used to synchronize the ground SAT clock to the GPS system time. To do this, the user receiver receives the normal GPS navigation signals and solves for time, one of the parameters available from GPS. The receiver need not be a very sophisticated GPS receiver in terms of capability. This is because it is stationary, i.e., no dynamics, and that it can use a long period of time to converge to a highly accurate solution. A good candidate receiver is a Manpack receiver of a Z set.

The oscillator shown in Figure 12 is a rubidium oscillator. The requirement for a high-quality oscillator stems from the fact that it may not be practical to simultaneously transmit the emulated GPS navigation signal and receive the normal GPS satellite signals at the same location. A possible trade-off is to remotely locate the GPS user receiver and antenna so that they would not be saturated by the emulated signal. A cable of known length would then be used to carry the time signal to the oscillator. This has the disadvantage of requiring two sites and the inherent reduction in site flexibility. Furthermore, with the approach wherein a stable oscillator is used to "coast" during

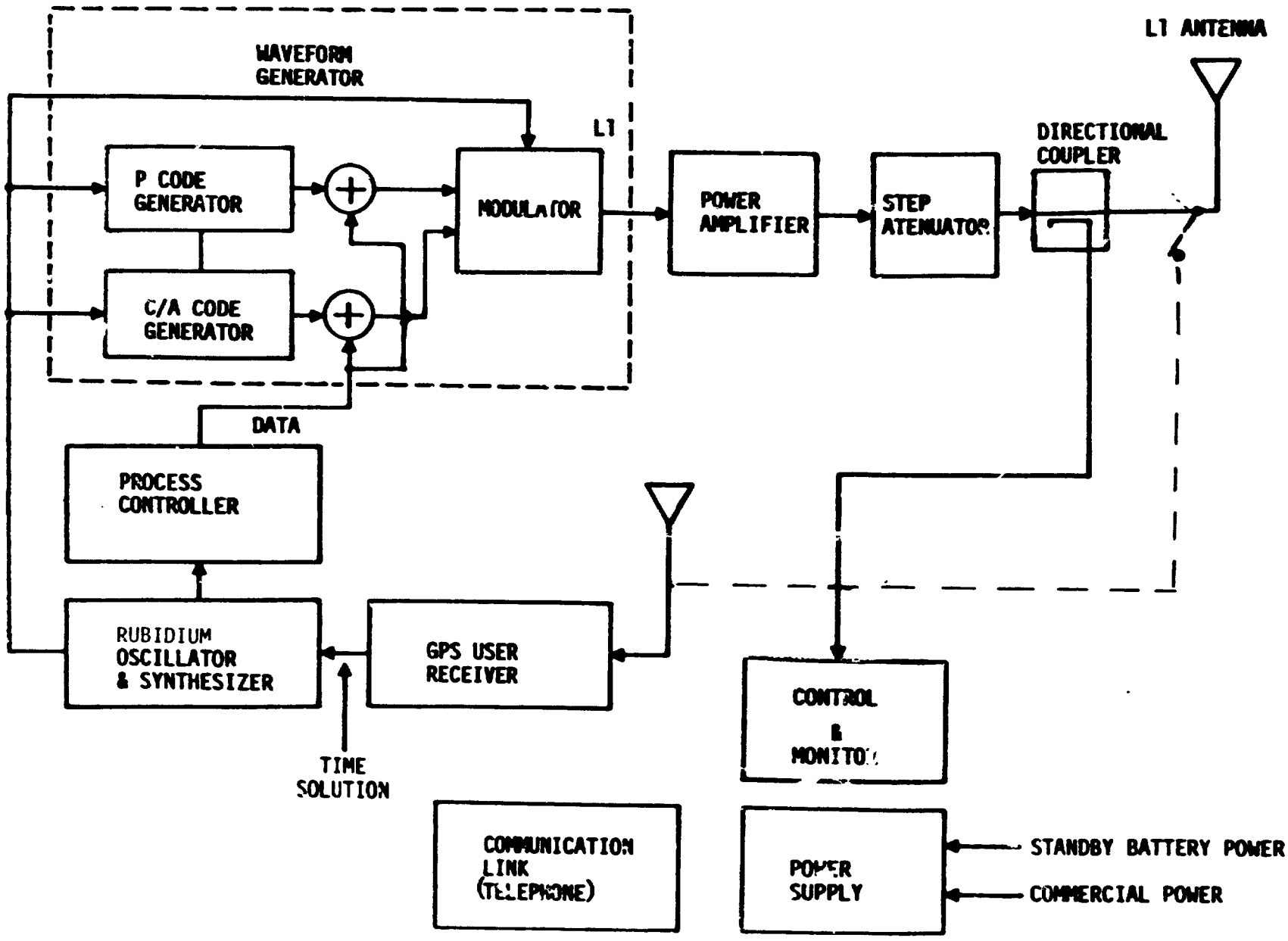

Figure 12. GPS Ground Transmitter for Shuttle Landing - Ground SAT

the transmission interval, one antenna with a suitable RF switch can be used for both transmit and receive functions. This is indicated by the dotted lines in Figure 12.

A summary of the specifications for a commercially available rubidium oscillator is given in Table 2. It can be seen that, with a short-term stability of $1x10^{-12}$ (τ=100 sec) and a long-term stability of $<1x10^{-11}$/month, this oscillator will provide excellent performance for the ground SAT application. The price of the oscillator is approximately $7000.

The ground SAT would be housed in a portable shelter such as that depicted in Figure 13. Figure 13 actually shows an existing ground transmitter used by the GPS Joint Program Office (JPO) for the Yuma GPS inverted range tests. A block diagram of this transmitter is shown in Figure 14. This block diagram contains all the elements shown in Figure 12, with the exception of the rubidium oscillator. The cost of the JPO ground transmitter has been reported by JPO to be approximately $100,000, including nonrecurring costs. Axiomatix estimates that the cost of a ground SAT for use with the Shuttle landing would be approximately $200,000. This would include the rubidum oscillator, the GPS user receiver, and redundant elements for critical signal paths.

The link budge for a ground SAT is given in Table 3. This budget is calculated for a 1 watt transmitter and includes 0.3 dB of antenna feed line loss. A range of 700 miles was arbitrarily chosen. The actual range will be less. A link margin of approximately 7 dB is obtained, which is more than adequate.

Table 2. Rubidium Oscillator Performance

	Model FRK-L	Model FRK-H
Output	10 MHz sine wave 0.5V rms into 50 ohms, floating ground OPTION 5 MHz, 1 MHz	
Signal to Noise (SSB 1 Hz BW)	>120 dB at 100 Hz and >145 dB at 1000 Hz from carrier	
Input Power	13W at 24 VDC, 25°C ambient; 22 to 32 VDC; peak current during warm-up, 1.8A	
Warm-up Characteristics	< 10 minutes to reach 2×10^{-10} at 25°C ambient	
Long Term Stability (Drift)	$< 4 \times 10^{-11}$/month	$< 1 \times 10^{-11}$/month
Short Term Stability	3×10^{-11} $\tau = 1$ sec 1×10^{-11} $\tau = 10$ sec 3×10^{-12} $\tau = 100$ sec	1×10^{-11} $\tau = 1$ sec 4×10^{-12} $\tau = 10$ sec 1×10^{-12} $\tau = 100$ sec
Trim Range	2×10^{-9}	1×10^{-9}
Environmental Effects		
Voltage Variation	$< 1 \times 10^{-11}$/10%	
*Operating Temperature	$<6 \times 10^{-10}$ from −40°C to +65°C OPTION $<1 \times 10^{-9}$ from −54°C to +65°C	$< 1 \times 10^{-10}$ from −25°C to +65°C OPTION $<4 \times 10^{-10}$ from −54°C +65°C
Storage Temperature	−54°C to +75°C	
Magnetic Field	$< 4 \times 10^{-11}$/Am^{-1} (3×10^{-11}/0.1 millitesla) Optional shield available	
Altitude	$< 1 \times 10^{-11}$/mbar (sea level to 21,000m)	
Humidity	95% MIL-T-5422F	
Shock	MIL-STD-810C, Method 516.2, Procedure I	
Vibration	MIL-STD-810C, Method 514.2, Procedure I	
General Information		
Size	100mm x 99mm x 112mm (3.9 in x 3.9 in x 4.4 in.)	
Weight	1.3 kg (2.9 lbs.), with optional heat sink EEK-10, 1.55 kg (3.5 lbs.)	
Electrical Protection	An internal diode and fuse protects against reversed polarity connection	
Connectors	Coaxial connector OSM 211, mates with OSM 501-3 or equivalent Eight push-on connector pins OPTION Winchester Connector PN SRE-20PJ, mates with SRE-20SJ	
Warranty	1 year, lamp and resonance cell-5 years	

*Operating temperature is baseplate temperature with optional heatsink EEK-10 attached. Highest operating temperature depends on heat transfer between heat sink and unit.

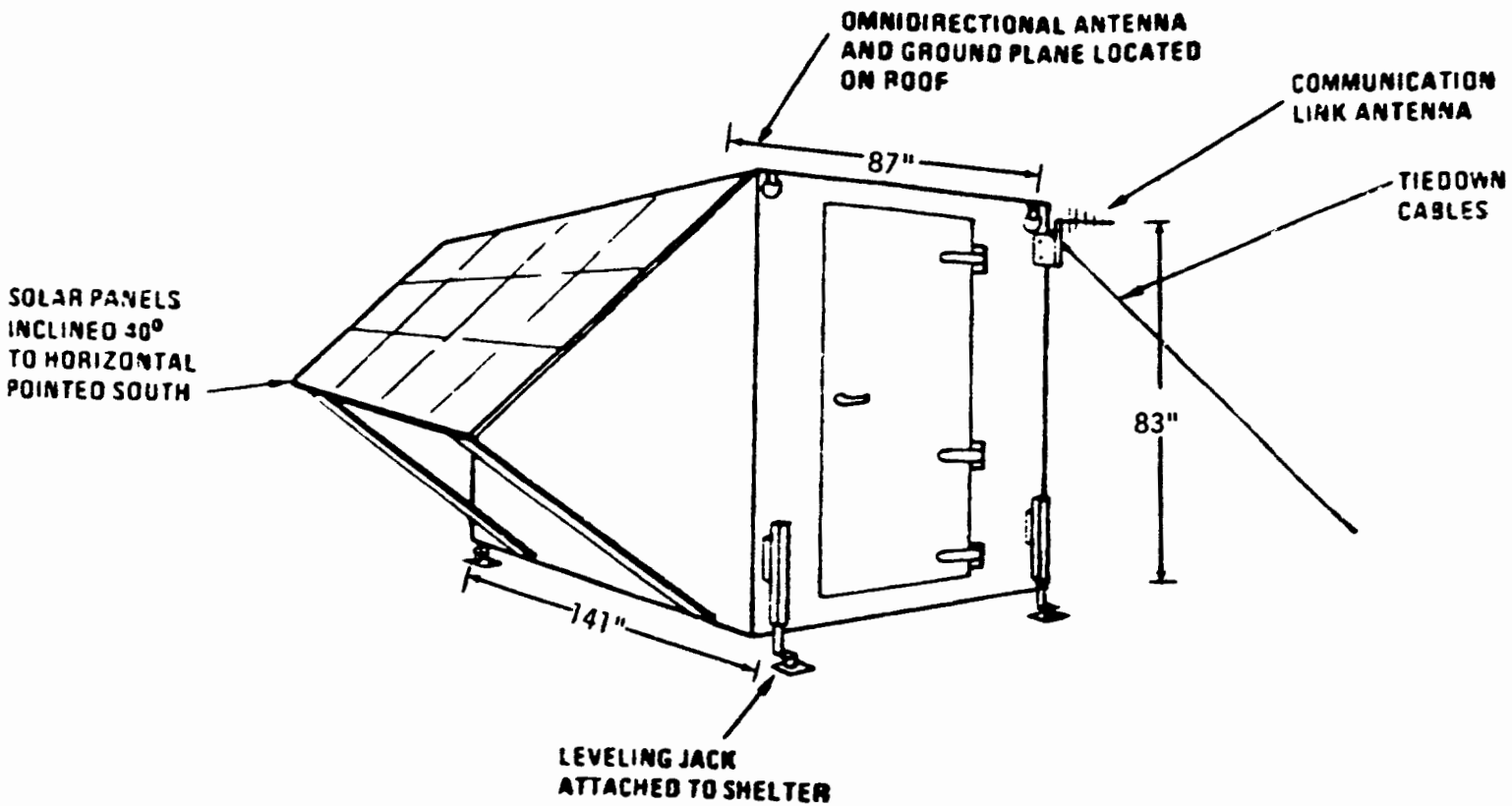

Figure 13. GPS Inverted Range Ground Transmitter

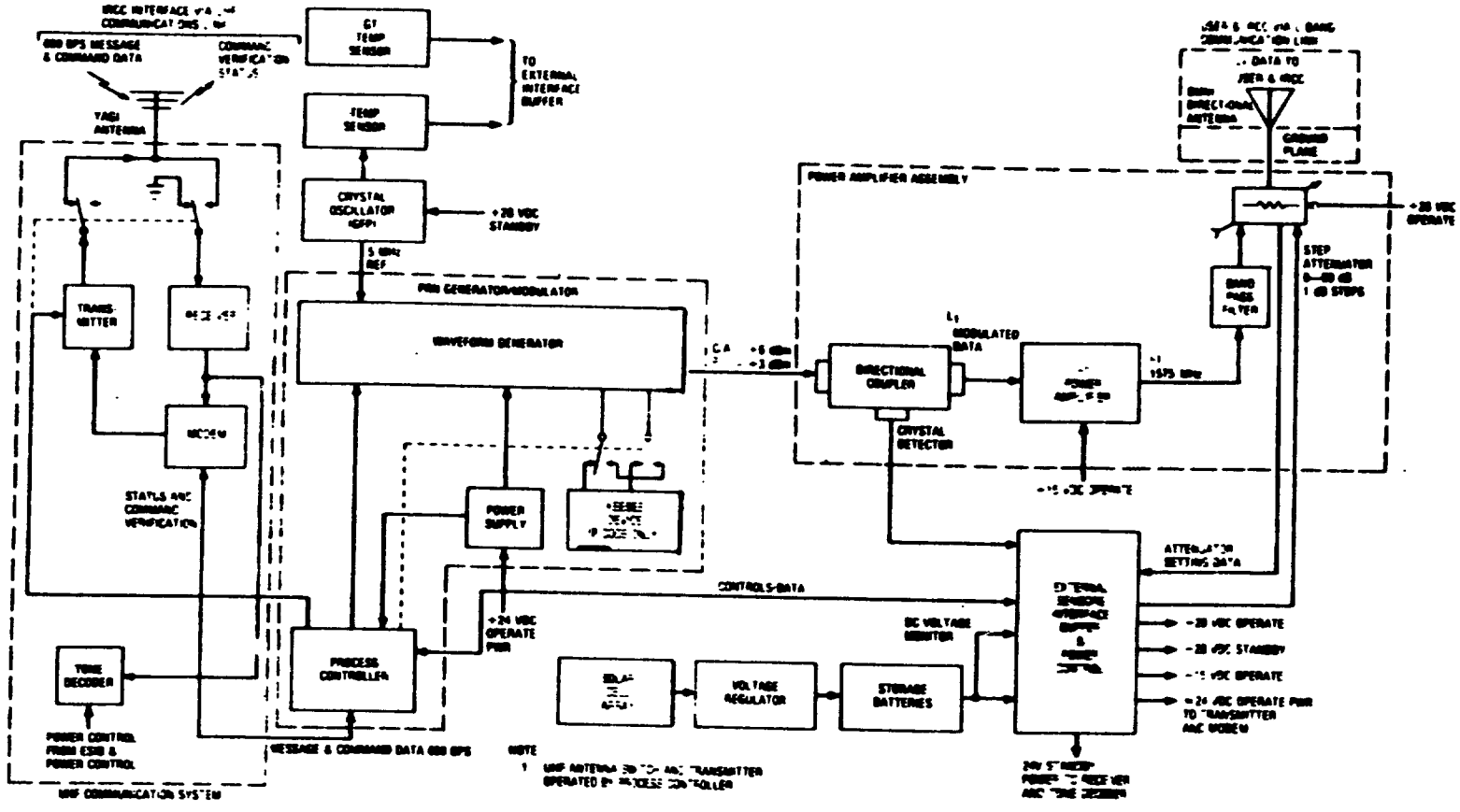

Figure 14. Ground Transmitter Block Diagram

ORIGINAL PAGE IS OF POOR QUALITY

Table 3. GPS Ground Transmitter/Shuttle Link L1-P

Transmitter Output Power at Antenna	- .3 dBW (1 watt transmitter)
Antenna Gain	- 3.0 dB
Space Loss	-153.5 dB (R = 700 miles)
Polarization and Atmospheric Loss	- 0.5 dB
Shuttle Antenna Gain	- 4.0 dB
Circuit Loss	- 1.0 dB
Received Power	-162.3 dBW
System Noise Temperature	27.5 dBK
Boltzman's Constant	-228.6 dB-W/K/Hz
Noise Spectral Density	-201.1 dB-W/Hz
C/N_0	35.8 dB
Required C/N_0 (Theoretical)	29.6 dB/Hz
Implementation Loss	2.0 dB
Required C/N_0	31.6 dB/Hz
Link Margin	7.2 dB

5.0 EFFECTS OF IONOSPHERIC DELAY MODELING ON GPS RECEIVER DESIGN

Radio waves which pass through the earth's ionosphere travel more slowly than in free space due to group retardation along the ray path. This retardation is proportional to the total number of free electrons encountered and, as a consequence, varies with the angle of the particular ray path, the time of day, time of year, and geographic location. The GPS navigation signals are likewise retarded by their propagation through the ionosphere. This retardation manifests itself as an error in the measured pseudo range, which is the basic observable for computation of the Shuttle's state vector with GPS. The approach taken to solve this problem has been to broadcast a navigation signal on two frequencies, L1 and L2, with the user receiver measuring pseudo range on both frequencies. Since the delay is proportional to the inverse of carrier frequency, the user receiver is able to calculate the absolute delay and thus accurately determine the pseudo range. This section examines the feasibility of accurately modeling the absolute ionospheric delay, thus eliminating the need for two frequencies. The impact on receiver design is examined along with the software impact to determine if there is a possible cost savings for the Shuttle GPS navigation system.

An RF signal propagating through the ionosphere is delayed by

$$\tau = \frac{K}{F^2}$$

where K is a parameter proportional to total electron content along the measurement path and F is the signal frequency. If we consider two frequencies, F_{L1} and F_{L2}, the delay on L1 is

$$\tau_{L1} = \frac{K}{F_{L1}^{\ 2}}$$

and the delay on L2 is

$$\tau_{L2} = \frac{K}{F_{L2}^{\ 2}}$$

The two-frequency receiver actually measures the differential delay between L1 and L2, $\Delta\tau$. This can be written as

$$\Delta\tau = \tau_{L1} - \tau_{L2} = \frac{K}{F_{L1}^{\ 2}} - \frac{K}{F_{L2}^{\ 2}}$$

Solving for K,

$$K = \Delta\tau\left(\frac{F_{L1}^{2}\,F_{L2}^{2}}{F_{L1}^{2}-F_{L2}^{2}}\right)$$

Thus

$$\tau_{L1} = \Delta\tau\left(\frac{F_{L2}^{2}}{F_{L1}^{2}-F_{L2}^{2}}\right)$$

This last equation demonstrates the principle of the two-frequency GPS receiver. However, the immediate interest is to determine whether the ionospheric delay can be modeled accurately enough to eliminate one of the frequencies.

The first ionospheric delay model studied is called the "slab thickness" model. It relates the delay to fOF2, the critical frequency of the F2 region of the ionosphere. The parameter fOF2 has been regularly measured for over 40 years by ionospheric sounders, called ionosondes. fOF2 is proportional to the electron density at the maximum of the F2 region, called N_{max}. A second parameter which has been measured for many years is MUF-F2, the maximum usable frequency of the F2 region, which has been shown to be closely related to the height of the maximum density of the F2 region. The ionospheric Total Electron Content (TEC), proportional to time delay, has been measured at only a few scattered locations via Faraday rotation effects. Klobuchar and Hawkins, however, have used available TEC data taken at Hamilton, Massachusetts, to form the ratio of TEC divided by N_{max}, which is called equivalent slab thickness. N_{max} values were obtained from fOF2 measurements made at Wallops Island, Virginia. This slab thickness ratio of two experimentally measured quantities is a first-order scale height or thickness parameter of the F2 ionospheric region. Thus, if a value of fOF2 is known, the ionospheric time delay can be obtained from

$$\Delta T = 1.67 \times 10^{-6}\tau\ \frac{(fOF2)^2}{F_{L1}^{2}} \quad \text{(seconds)}$$

where fOF2 is in MHz, τ comes from the slab thickness model and is expressed in km, and F_{L1} is the GPS L1 carrier frequency.

A model for τ was derived from the existing measured data.

A model value of τ is determined from

$$\tau = \tau(h, M, F10.7) = [M(\text{month})^* F\ 10.7 + B(M)]\ {}^*C(h, M)$$

where h is the hour of the day, M is the month of the year, and 10.7 is the 10.7 cm solar flux coefficient for a linear fit. These model coefficients are tabulated in Table 4.

The error in this slab thickness model is shown plotted in Figure 15. The error is greatest, approximately 10%, during the night hours since the total ionospheric delay is least at these times. Conversely, the error is smallest, 5%, during midday when, due to the additional ionization caused by the sun, the ionospheric delay is greatest. Thus, it might be concluded that this is an excellent model; however, the serious drawbacks for this model are as follows: the model is appropriate only for a restricted geographic locale and, since approximately 4 kilobits of computer storage are required for the model, excessive computer storage would be required for a worldwide model. Furthermore, the research to extend the model to a worldwide basis has yet to be performed.

Several models of ionospheric delay have been developed by The Johns Hopkins University Applied Physics Laboratory. An example of these models is an algorithm in which the ionospheric group delay is obtained via ray-tracing based on a priori estimates of the electron density distribution. The ionospheric group time delay is given to the first order as

$$\tau(G, t) = \frac{1.34 \times 10^2}{F_{L1}^{\ 2}} \int_{G(t)} N(\vec{r}, t)\, ds$$

where

$\tau(G, t)$ = ionospheric group time delay of the ranging signal between satellite and navigator along the geometric path G(t) at time t, ns

f = carrier frequency, Hz

$N(\vec{r}, t)$ = electron density at $\vec{r}$ and t, electrons/m^3

$\vec{r}$ = position vector to a point on G(t)

ds = differential element of arc along G(t), m

A vertical electron density profile is used to characterize the electron density distribution. The model for this is shown in Figure 16. This model is characterized by 11 parameters, each of which can be a function of geographic location, time, solar activity, etc. The 11

ORIGINAL PAGE IS
OF POOR QUALITY

Table 4. Slab Thickness Model Coefficients

AFCRL MID-LATITUDE SLAB THICKNESS MODEL COEFFICIENTS

NO.	F10.7 COEFF. M	F10.7 COEFF. B	LOCAL HOUR 0	1	2	3	4	5	6	7	8	9	10	11	12	13	14	15	16	17	18	19	20	21	22	23
1	-169	2[illegible]9.	1.15	1.09	1.[illegible]	1.05	1.08	1.01	.98	.84	.73	.87	.82	.83	.98	.95	.9[illegible]	.93	.99	.98	1.00	.98	1.12	1.24	1.32	1.2
2	.259	214.	1.12	1.09	1.[illegible]	1.07	1.07	1.[illegible]	1.0[illegible]	.82	.76	.31	.87	.91	.95	.98	1.00	1.00	1.00	.98	.99	1.02	1.02	1.11	1.11	1.1
3	.184	228.	1.32	1.02	1.[illegible]	1.12	1.14	1.[illegible]	1.0[illegible]	.84	.65	.91	.99	.98	.99	1.[illegible]	1.03	1.03	1.04	1.01	.99	1.03	1.02	1.03	1.03	1.0
4	.1[illegible]	253	.92	.9[illegible]	.9[illegible]	.98	.91	.93	.93	.9[illegible]	1.00	1.09	1.09	1.12	1.00	1.07	1.07	1.05	1.07	1.07	1.0[illegible]	.96	.98	1.00	.98	.9
5	.2[illegible]9	273.	.8[illegible]	.8[illegible]	.8[illegible]	.87	.93	1.0[illegible]	1.01	1.02	1.07	1.08	1.12	1.1[illegible]	1.12	1.09	1.08	1.09	1.07	1.07	1.02	.95	.93	.91	.89	.8
6	1.121	168.	.92	.82	.83	.97	.92	1.08	1.06	1.0[illegible]	1.07	1.[illegible]	1.11	1.1[illegible]	1.12	1.14	1.14	1.14	1.13	1.07	1.[illegible]	.97	.98	.85	.85	.8
7	.0[illegible]1	186	.85	.8[illegible]	.8[illegible]	.98	.9[illegible]	1.09	1.0[illegible]	1.0[illegible]	1.0[illegible]	1.0[illegible]	1.06	1.10	1.12	1.13	1.1[illegible]	1.14	1.13	1.10	1.05	.90	.89	.86	.85	.8
8	.552	289.	.81	.9[illegible]	.89	.89	.89	.98	.56	.98	.95	.99	1.0[illegible]	1.0[illegible]	1.11	1.12	1.1[illegible]	1.1[illegible]	1.13	1.16	1.11	.98	.92	.90	.91	.9
9	.2[illegible]5	157.	1.0[illegible]	.9[illegible]	.9[illegible]	.97	.99	.99	.9[illegible]	.9[illegible]	.87	.54	.9[illegible]	1.[illegible]	1.0[illegible]	1.0[illegible]	1.0[illegible]	1.0[illegible]	1.08	1.06	1.0[illegible]	1.01	1.03	1.04	1.03	1.3
10	.329	193.	1.08	1.07	1.06	1.05	1.0[illegible]	1.0[illegible]	.69	.7[illegible]	.88	.95	.93	.97	.99	.99	.98	.97	.9[illegible]	.96	1.03	1.12	1.13	1.16	1.12	1.1
11	.[illegible]19	17[illegible].	1.1[illegible]	1.19	1.1[illegible]	1.07	1.0[illegible]	1.0[illegible]	1.12	.76	.71	.78	.81	.89	.88	.88	.89	.9[illegible]	.89	.95	1.08	1.07	1.18	1.23	1.24	1.1
12	.37[illegible]	199.	1.22	1.1[illegible]	1.07	1.01	1.01	1.03	1.08	.78	.71	.7[illegible]	.88	.81	.8[illegible]	.8[illegible]	.89	.91	.98	.9[illegible]	1.0[illegible]	1.08	1.23	1.28	1.32	1.2

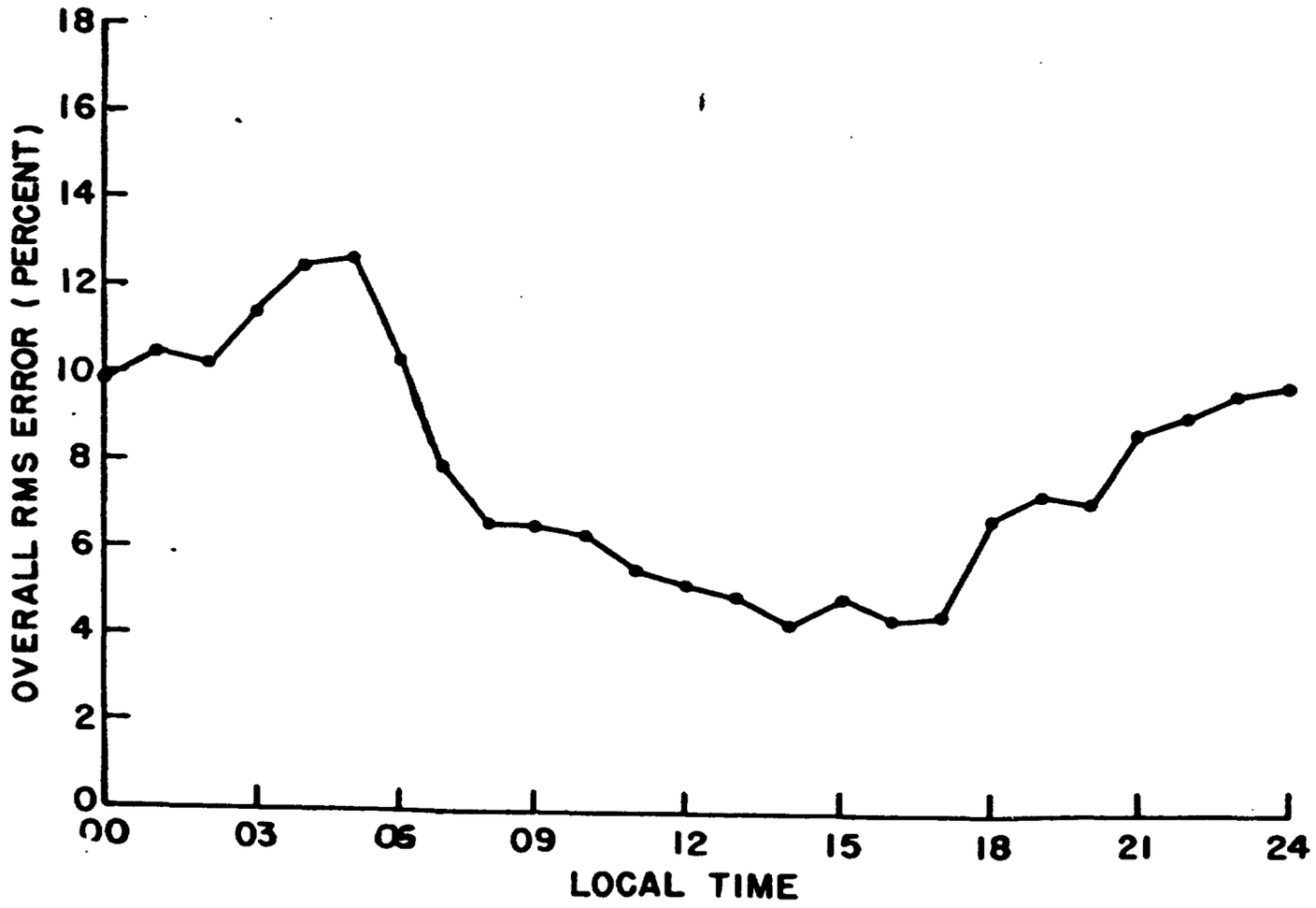

Figure 15. Error in Slab Thickness Model

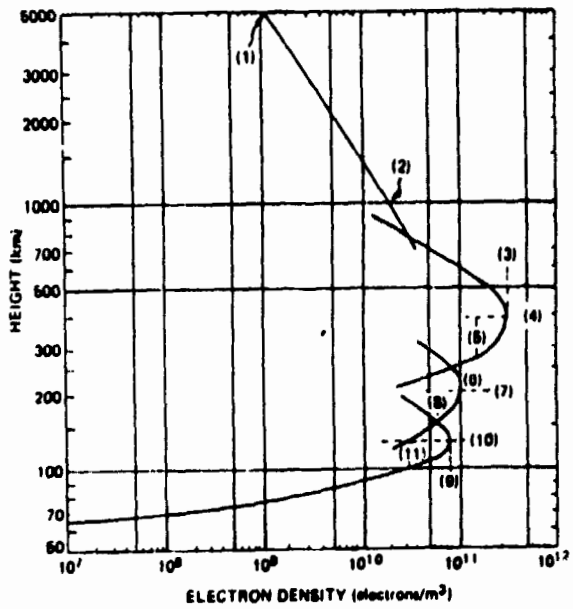

ORIGINAL PAGE IS
OF POOR QUALITY

Figure 16. Eleven-Parameter Vertical Electron Density Profile

parameters are determined in the following manner:

(1) Density at 5000 km--an analytical function of the month of the year and the gyrofrequency.

(2) Density at 1000 km--an analytical function of magnetic dip and solar zenith angle.

F2 region

(3) Maximum electron density--obtained as a function of geographic location, universal time, month, and solar index from predictions of fOF2 available from NOAA.

(4) Height of the maximum--obtained as a function of geographic location, universal time, month, and solar index from predictions of M(3000)F2 available from NOAA.

(5) Semithickness--obtained as a function of geographic location, universal time, month, and solar index from predictions of hmF2/ymF2 available from NOAA.

F1 region

(6) Maximum electron density--obtained as a function of solar index and solar zenith angle from an empirical formula.

(7) Height of maximum--obtained as a function of solar zenith angle from an empirical formula.

(8) Semithickness--constant at 50 km.

E region

(9) Maximum electron density--obtained as a function of geographic location, universal time, month, and solar index from predictions of fOE available from NOAA.

(10) Height of maximum--constant at 130 km.

(11) Semithickness--constant at 20 km.

The residuals for this, along with two other APL algorithms, are shown plotted for three locations in Figure 17. It can be seen that the residuals are on the order of 10 nanoseconds, which is an excellent result. As far as applying this model to Space Shuttle GPS navigation, however, there is the problem of gathering all the pertinent parameters discussed above, for a wide geographic area and time, and storing the data in the GPS receiver computer. Thus, the two-frequency receiver hardware penalty must be examined in light of this software penalty.

The major impact on GPS receiver design of two-frequency, L1/L2,

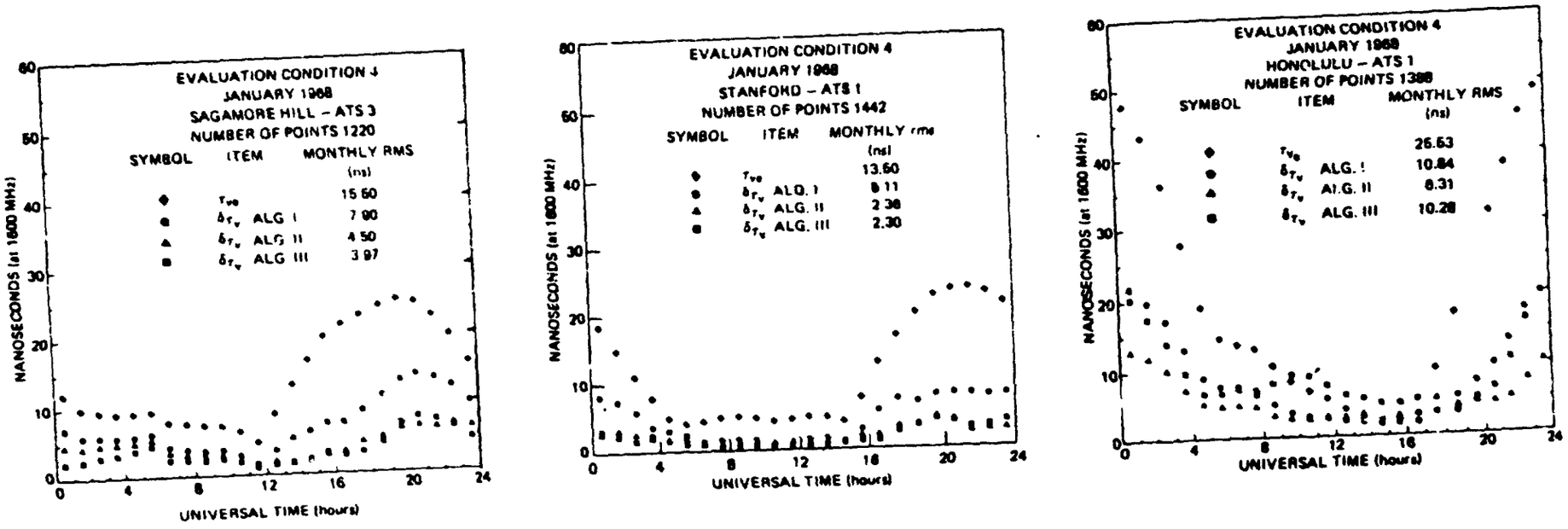

Figure 17. APL Ionospheric Model Residuals

ORIGINAL PAGE IS
OF POOR QUALITY

operation is in the front-end down-converter and in the receiver frequency synthesizer. Substantial increases in receiver complexity are avoided by time multiplexing the receiver RF, IF, and baseband processing between the L1 and L2 frequencies. Figure 18 shows a typical RF front-end and down-converter design for a two-frequency receiver. The increased complexity due to L1 and L2 frequencies is shown by the dotted lines. The frequency synthesizer for the same typical GPS receiver design is shown in Figure 19. Again, the increased complexity due to L1/L2 operation is indicated by the dotted lines. The added complexity for L1/L2 operation, relative to the overall receiver complexity, is slight. When compared with the research, software, and computer firmware required to implement a suitable ionospheric delay model, the conclusion is reached to retain the two-frequency approach for the Shuttle GPS receiver.

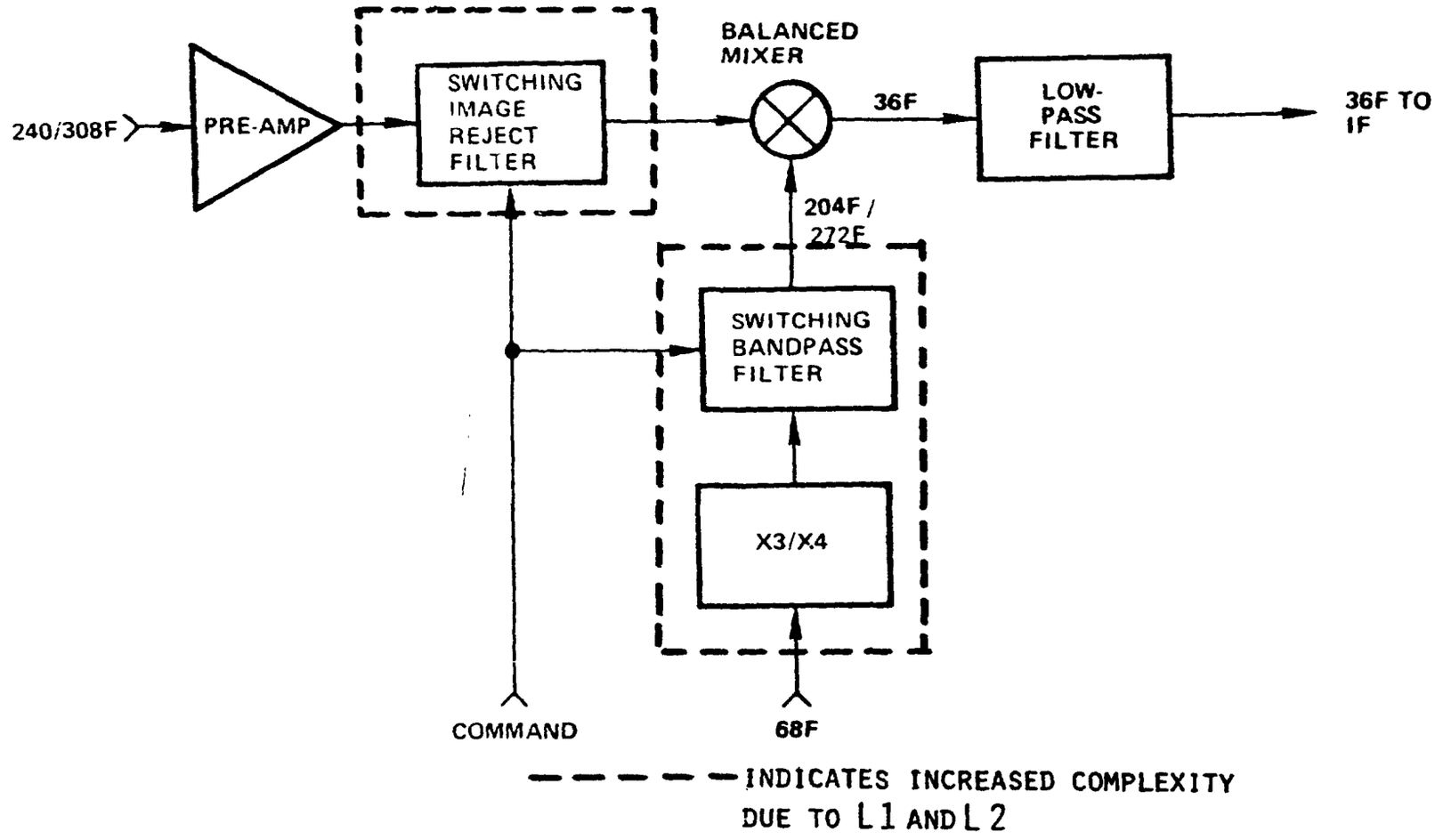

Figure 18. Front-End and Down-Converter for Two-Frequency Receiver

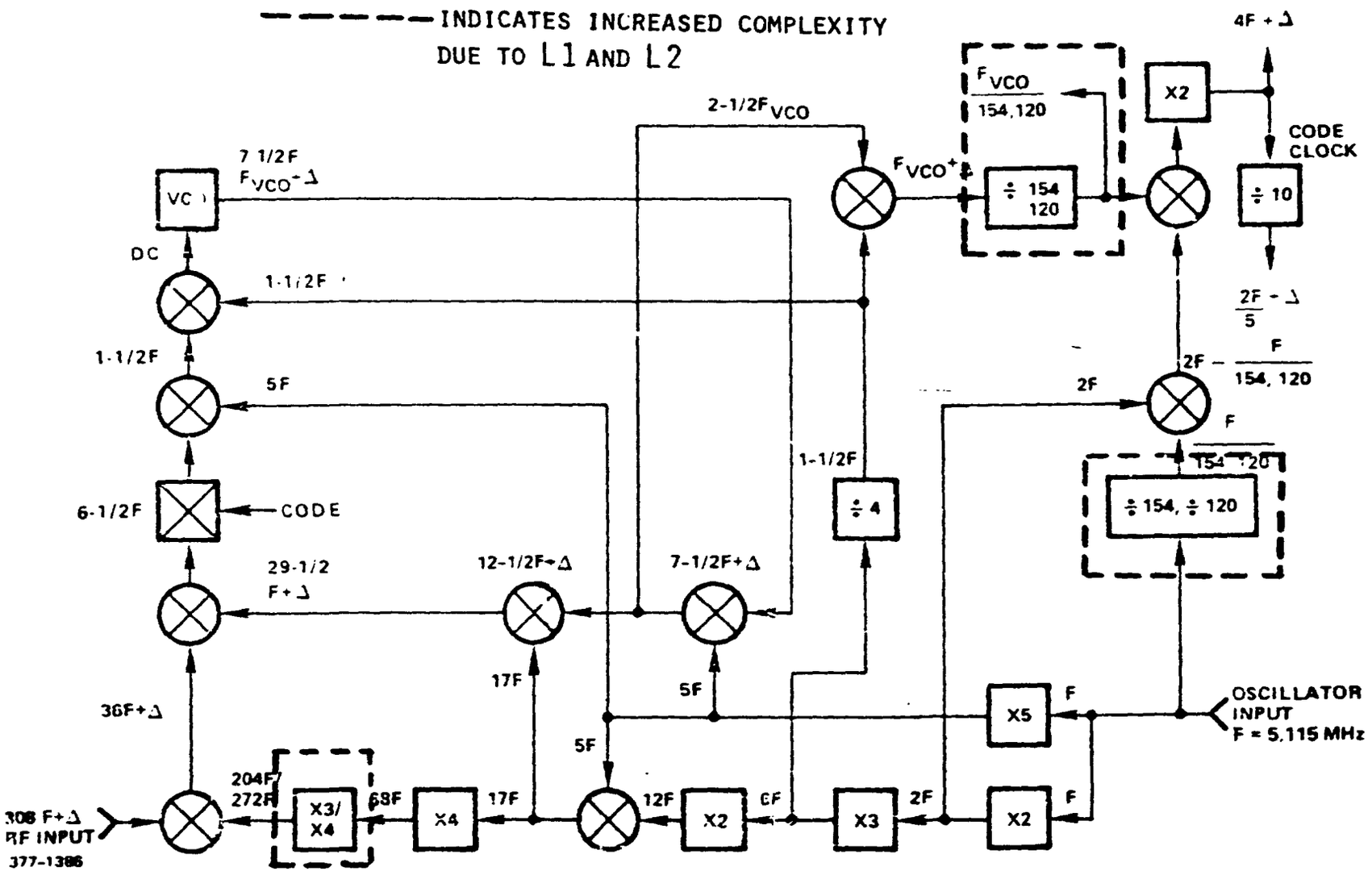

Figure 19. Typical RF Frequency Plan for Two-Frequency Receiver Synthesizer

6.0 GPS RECEIVER TRACKING OF SHUTTLE TRANSIENT MANEUVERS

The Shuttle GPS receiver tracking loops must be sufficiently narrowband so that the tracking error due to thermal noise is small. However, this situation generally presents the classic coherent receiver trade-off between loop noise performance and dynamic maneuver tracking capability. That is to say, a narrowband loop is desirable from a noise consideration, and a wideband loop is desirable from a dynamic tracking consideration. The analysis which follows examines the dynamic tracking performance for the GPS receiver carrier and code loops. Typical values of bandwidth are used and the dynamics used are typical Orbiter on-orbit maneuvers.

The acceleration rate, or jerk, profiles for an Orbiter pitch maneuver start and an OMS burn are shown in Figure 20. These profiles have been modeled as pulses, as shown by the dotted line in Figure 20. Although this is a worst-case model, it is analytically tractable.

The tracking loops for both the carrier loop and the code loop are taken as second-order phase lock loops. The loop transfer function for the second-order phase lock loop is given by

$$\frac{\hat{\theta}(s)}{\theta(s)} \triangleq H(s) = \frac{1 + \left(\frac{r+1}{2W_L}\right) s}{1 + \left(\frac{r+1}{2W_L}\right) s + \frac{1}{r}\left(\frac{r+1}{2W_L}\right)^2 s^2}$$

where

$r = AK\,\tau_2\,F_0$

$F_0 = \tau_2/\tau_1$

ζ = loop damping factor = $\sqrt{r}/2$

ω_n = loop natural frequency = $\sqrt{r}/\tau_2$

W_L = two-sided noise bandwidth = $(r+1)/2\tau_2$

The loop error transfer function is given by

$$\frac{\phi(s)}{\theta(s)} = \frac{\theta(s) - \hat{\theta}(s)}{\theta(s)} = 1 - H(s) = \frac{\frac{1}{r}\left(\frac{r+1}{2W_L}\right)^2 s^2}{1 + \left(\frac{r+1}{2W_L}\right) s + \frac{1}{r}\left(\frac{r+1}{2W_L}\right)^2 s^2}$$

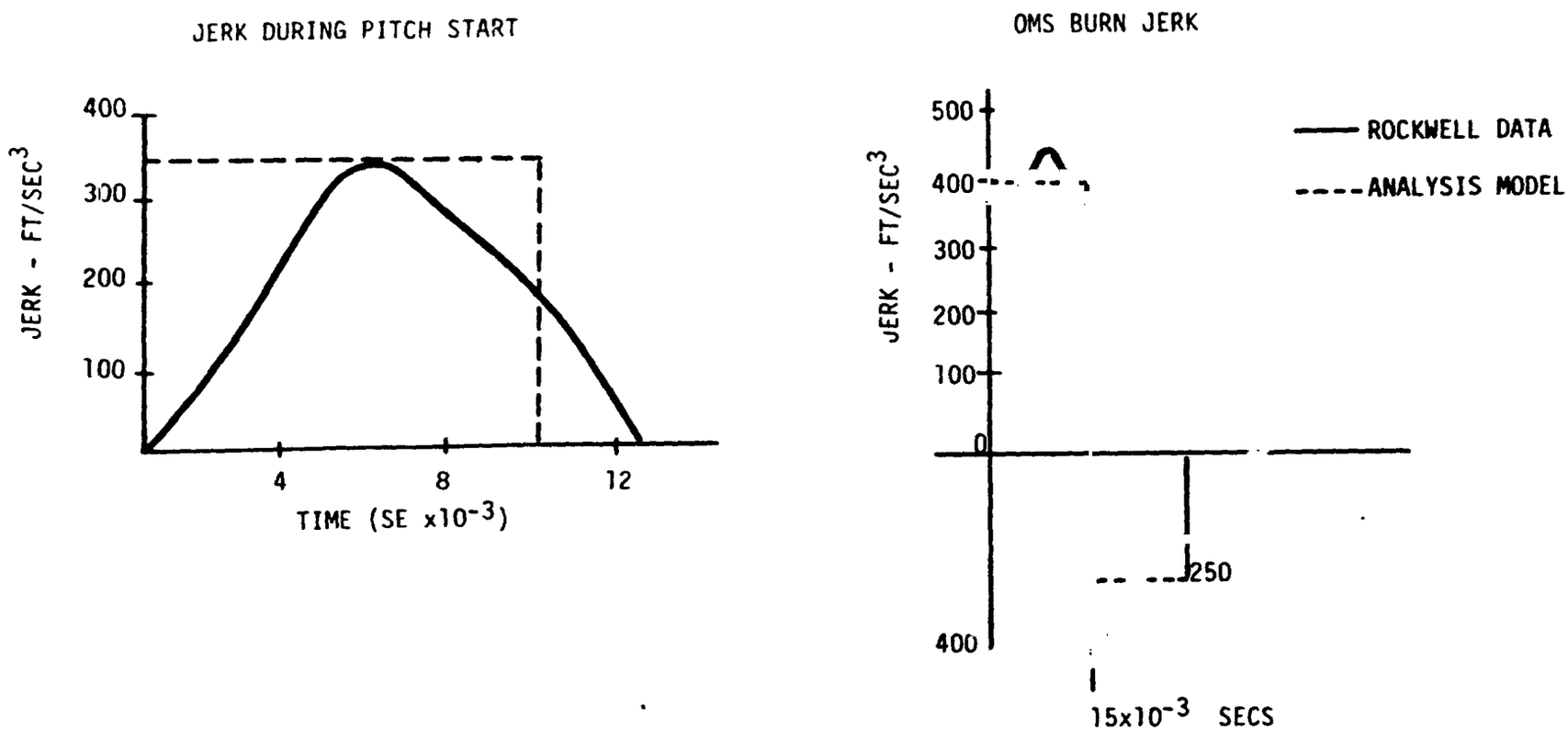

Figure 20. Jerk Models for Receiver Transient Performance Evaluation

A pulse in jerk in the time domain is given by

$$\theta(t) = \dddot{\theta}\,\frac{t^2}{6}\,u(t) - \dddot{\theta}\,\frac{(t-t_1)^3}{6}\,u(t-t_1)$$

where u(t) is the unit step function and

$$\dddot{\theta} = \frac{\dot{a}}{c}\,f_0$$

where

$\dot{a}$ = acceleration rate or jerk in ft/sec.^{3}

c = propagation velocity in ft/sec.

f_0 = carrier frequency in the case of the carrier loop (~1.6×10^9 Hz)

= P code rate in the case of the code loop (~1×10^7 Hz)

In the s domain (Laplace transform), the pulse in jerk is given by

$$\theta(s) = \frac{\dddot{\theta}}{s^4}\,[1 - e^{-st_1}]$$

The approach taken here will be to solve for the time response for a step in jerk (i.e., ignore the e^{-st_1} term) and then use superposition to get the pulse response by subtracting the step response at $t = t_1$. The phase error, in the s domain, for the step in jerk is found to be

$$\phi(s) = \frac{\frac{A^2}{r}\dddot{\theta}}{s^2} - \frac{\frac{A^3}{r}\dddot{\theta}}{s} + \frac{\frac{A^4}{r}\left(1 - \frac{1}{r}\right)\dddot{\theta} + \frac{A^5}{r^2}\dddot{\theta}\,s}{1 + As + \frac{A^2}{r}s^2}$$

where $A = \frac{r+1}{2W_L}$

The inverse transform is first found for the case of critical damping; i.e., $\zeta = 1$

$$\phi(t) = \frac{\dddot{\theta}}{B_L^{\,3}}\left[\frac{25}{64}B_L t\left(1+\exp(-\tfrac{8}{5}B_L t)\right) - \frac{125}{256}\left(1-\exp(-\tfrac{8}{5}B_L t)\right)\right]u(t)$$

The more interesting case is for $\zeta = 0.707$, for which we find

$$\phi(t) = \left(\frac{\dddot{\theta}}{B_L^{\,3}}\right)\frac{9}{32}\left[B_L t - \frac{3}{4}\left(1-\exp(-\tfrac{4}{3}B_L t)\cos\tfrac{4}{3}B_L t\right)\right]u(t)$$

Since this is the response to a step in jerk, the pulse response is found from superposition by using

$$\phi(t)_{pulse} = \phi(t)\ u(t) - \phi(t-t_1)\ u(t-t_1)$$

The normalized second-order loop error response for both a step input of jerk and a pulse input (10 msec wide) are shown plotted in Figure 21. It can be seen from the figure that, for a step long enough in duration, the loop error will grow to the point where the loop breaks lock. For a pulse input, the loop error reaches a steady-state value that is proportional to the inverse of B_L^3. Thus, the desire for wider tracking bandwidths to accommodate dynamic tracking can be seen.

The GPS carrier loop and code loop errors for the Shuttle pitch start jerk input are shown plotted in Figure 22. The code loop bandwidth of $B_L = 1$ Hz has purposely been chosen to be somewhat narrower than the actual case to accomplish a worst-case evaluation. Even so, the code loop error is seen to be only 10^{-2} P code chips, or about 1 ft. This error is insignificant. The carrier loop bandwidth of 10 Hz is also somewhat narrow for purposes of worst-case evaluation. Even so, the carrier loop error is seen to be only about 10^{-3} radians. This error is totally insignificant. Thus, it is concluded that typical on-orbit maneuvers do not affect the GPS receiver tracking performance.

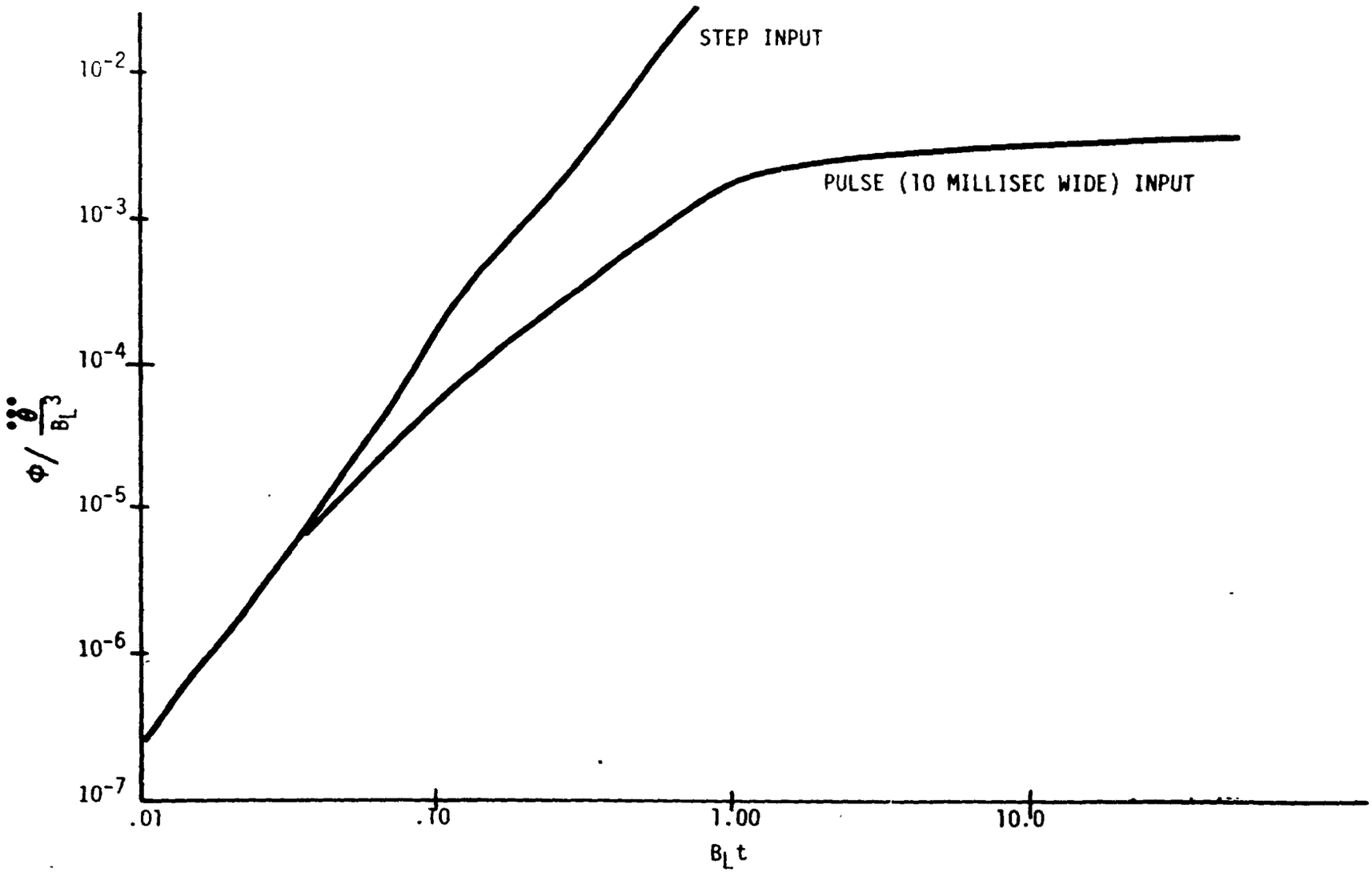

Figure 21. Error Response for 2nd Order Phase Lock Loop with Acceleration Rate (Jerk) Input

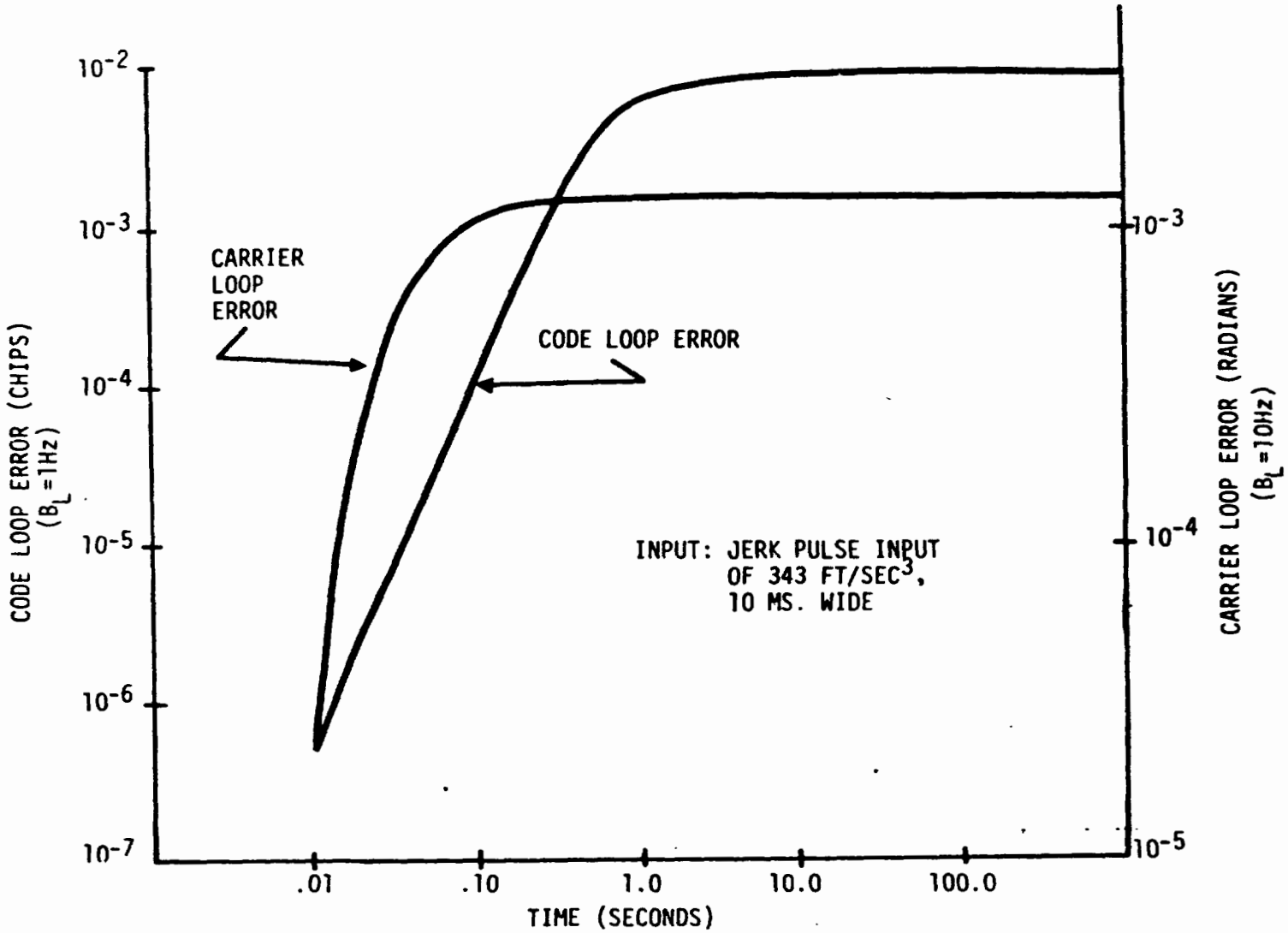

Figure 22. GPS Receiver Tracking Loop Response to Shuttle Transient Maneuver

REFERENCES

1. Blanchard, A. Phase-Locked Loops, Application to Coherent Receiver Design. John Wiley & Sons, 1976.

2. Spilker, J. J. Digital Communications by Satellite. Prentice-Hall, Inc., 1977.

3. Gradshteyn, I. S., and I. W. Ryzhik. Tables of Integrals Series and Products. Academic Press, 1965.